Energy Storage Using Osmotic Processes: A Thermodynamics Based Model

by

Adam Vickerman
B.Sc., Massachusetts Institute of Technology, 2013

A Project Report Submitted in Partial Fulfillment of the
Requirements for the Degree of

MASTER'S OF ENGINEERING

in the Department of Mechanical Engineering

ABSTRACT

Reliable, economic and efficient energy storage is needed to help shift from primarily fossil fuel generated electricity to clean energy. This report develops a thermodynamics based model for an osmotic energy storage (OES) system. This system uses reverse osmosis (RO) to store energy and pressure retarded osmosis (PRO) to produce power during the discharge cycle. Bottom up RO and PRO models were created in MATLAB for hollow fiber membrane modules. These models were then used in an overall OES system model. Preliminary results were produced, with a maximum round trip efficiency of 8.97%. Note that operating conditions were not optimized, and higher efficiencies can be achieved using the model developed here. Salt leakage plays a large role in limiting system efficiency.

Contents

List of Tables

List of Figures

List of Symbols

Name	Symbol	Units
Efficiency	η	-
Work	W	J
Osmotic pressure	π	Pa
Pressure differential	Δp	Pa
Molar chemical potential	$\bar{\mu}$	J/mol
Temperature	T	K
Pressure	p	Pa
Molar Gibbs free energy	$\bar{g}$	J/mol
Molar volume	$\bar{\nu}$	m^3/mol
Mole fraction	X	-
Molar gas constant	$\bar{R}$	J/mol-K
van't Hoff factor	i	-
Activity coefficient	γ	-
Molar flux	$\bar{J}$	mol/m^2-s
Transport coefficient	$\bar{L}$	mol^2/J-m-s
Water flux	J^w	m/s
Water permeability coefficient	A	m/s-Pa
Salt flux	J^s	kg/m^2-s
Salt permeability coefficient	B	m/s
Concentration	C	kg/m^3
Diffusion coefficient	D_s	m^2/s
Boundary layer width	δ	m
External CP mass transfer coefficient	k	m/s
Membrane support layer porosity	ϵ_m	-
Internal CP mass transfer coefficient	K	s/m

Membrane support layer tortuosity	τ	-
Membrane support layer thickness	t	m
Membrane support layer structure factor	S	m
Entropy of mixing	S_{mix}	J/K
Moles of species α	n_α	mol
Active module length	L_{mem}	m
Active module radius	R	m
Central tube radius	R_c	m
Void fraction	ϵ	-
Fiber outer diameter	$d_{f,o}$	m
Fiber inner diameter	$d_{f,i}$	m
Density	ρ	kg/m^3
Dynamic viscosity	μ	Pa-s
Axial length of cells	Δz	m
Number of axial divisions	N_z	-
Radial length of cells	Δr	m
Number of radial divisions	N_r	-
Total active membrane area	$A_{m,T}$	m^2
Membrane area per volume	A_m	1/m
Total number of fibers	n	-
Number of fibers per cell	n_c	-
Mass flow rate	$\dot{m}$	kg/s
Volumetric flow rate	$\dot{V}$	m^3/s
Salinity	s	kg/kg
Superficial velocity	v	m/s
Sherwood number	Sh	-
Reynold's number	Re	-
Schmidt number	Sc	-
Velocity	u	m/s
Molar concentration	$\bar{C}$	mol/m^3
Error	e	-
Power	$\dot{W}$	J/s
Mixing ratio	M	-
Recovery ratio	RR	-

Chapter 1

Introduction

One of the key technology advancements required for the shift from primarily fossil fuel generated electricity to clean energy is the development of reliable, economic and efficient energy storage. A novel osmotic energy storage (OES) system was proposed by Bharadwaj & Struchtrup [5]. In this system reverse osmosis (RO) is used to separate saltwater into freshwater and a concentrated brine, storing energy, and pressure retarded osmosis (PRO) is used to harness the energy of mixing upon recombining these two streams, effectively discharging this battery.

In their paper *Large scale energy storage using multistage osmotic processes: Approaching high efficiency and energy density* [5], Bharadwaj & Struchtrup find that OES has the potential to provide energy storage at reasonable efficiencies and similar energy densities to that of pumped hydro storage. However, many simplifying assumptions were used and a more rigorous approach is required to adequately assess the promise of this energy storage technology.

This report details the implementation of a thermodynamics based model that can be used to explore the operating conditions and potential efficiencies of an OES system in more detail. This model is then used to produce preliminary results and begin to analyze the performance of an OES system.

Chapter 2

Background

2.1 Osmotic Pressure

The first concept required to understand the phenomena at work in an OES system is osmotic pressure. Neglecting density, charge and other differences, the natural state of a mixture of two substances is to be uniformly mixed. This can be seen when putting a drop of dye in water: it naturally diffuses and soon the solution is one uniform colour. Similarly, if pure water is put in contact with saltwater, they tend to mix together until a uniform concentration is achieved.

If a membrane that allows water to pass but not salt is placed between saltwater and pure water, the pure water will cross the membrane to dilute the saltwater, creating a mixture of uniform concentration. This can, however be prevented by pressurizing the saltwater. The pressure differential at which saltwater and pure water are in equilibrium and no water is passing across the membrane in either direction is called the osmotic pressure.

2.2 Osmotic Processes

The two osmotic processes that will be discussed in this report function due to osmotic pressure. They are reverse osmosis (RO) and pressure retarded osmosis (PRO). Both are membrane based processes and the focus throughout this report will be on saltwater as a working fluid.

Reverse osmosis is the predominant method of freshwater production from seawater. The traditional method of freshwater production was to use thermal processes.

Advances in membrane based technology have made thermal processes largely obsolete in mass production of freshwater as RO requires significantly less energy. RO is widely used and well understood. It is performed by pressurizing seawater above its osmotic pressure and putting it in contact with a membrane designed for RO. This elevated pressure will cause water to pass through the membrane, while the membrane restricts salt flow. The process results in two outflowing streams: a concentrated, high salinity brine, and low salinity freshwater.

Pressure retarded osmosis is the opposite process. It is a method of harnessing the energy of mixing of high salinity brine and low salinity freshwater. The high salinity brine is pressurized, but to a level below the fluid's osmotic pressure. The pressurized brine is then put in contact with a membrane that has low salinity freshwater on its other side. Since the hydrostatic pressure differential is lower than the osmotic pressure differential, freshwater will pass through the membrane to the high pressure brine side. Resulting from this process, the outgoing flow of high pressure fluid will be larger than the incoming flow of high pressure brine. This outgoing high pressure fluid can be run through a turbine to produce power. Since the outgoing flow is larger than the incoming flow, at a similar pressure, this process has the potential to generate net positive power. The pressures required to pump the freshwater are much lower than that of the brine and as such will only slightly decrease the net power produced.

Fig. 2.1 shows a conceptual design of a PRO system [1]. If the membrane is ignored, the height of the pressure chamber will balance the pressure provided by the pump and no water will flow. However, if the water is pressurized to a level below the osmotic pressure of the seawater then freshwater will pass through the membrane. Since more water is entering the pressure chamber, it will flow out the top and down onto the waterwheel. If the pressures and freshwater flow rates are sufficient, the water wheel will provide enough power to run the pump with the remainder being transformed to electricity by the generator. This basic concept is applied in modern PRO, except a turbine is used to harness the energy of the pressurized water instead of a waterwheel and generator.

2.3 Osmotic Energy Storage Efficiency

RO and PRO can be used together to create an OES system. One key metric for evaluating such a system is the round trip efficiency of the storage technology. For

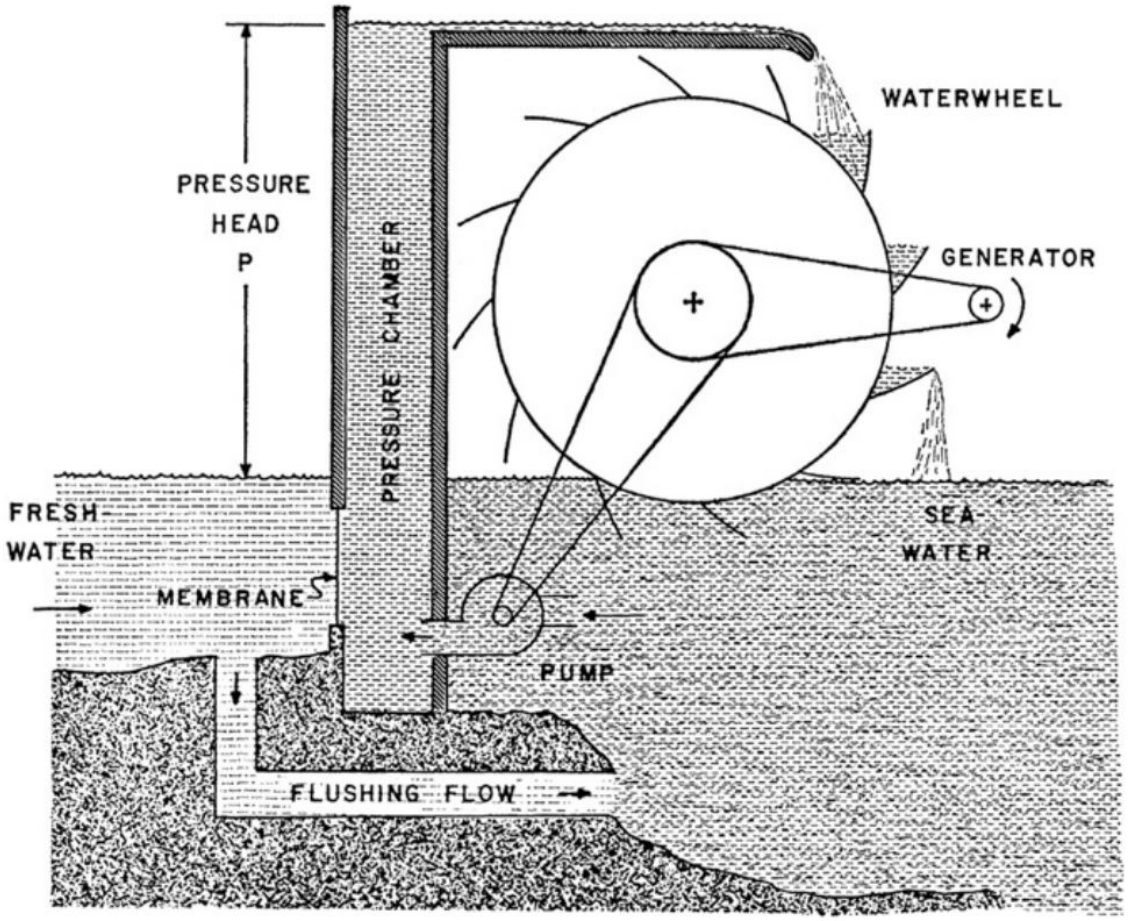

Figure 2.1: A conceptual pressure retarded osmosis system. (Reprinted from [1])

an OES system this efficiency, η_{OES}, can be calculated as:

$$\eta_{OES} = \frac{W_{PRO}}{W_{RO}} = \frac{\sum W_{PRO}^{T} - \sum W_{PRO}^{P}}{\sum W_{RO}^{P}}, \tag{2.1}$$

where W_{PRO} is the net work produced by the PRO stage and W_{RO} is the work required for the RO stage. W^T is the work produced by the turbine and W^P is the work required for a pump, with the subscripts referring to the stage in which the device is working. In an ideal system, the efficiency would be 1, or 100%. All energy put into separating freshwater and brine (RO) would be recovered during mixing (PRO). In reality this value will be between 0 and 1. For a point of reference, pumped hydro has round trip efficiencies of 70-85% [5].

2.4 Previous Work

A novel OES system was proposed by Bharadwaj & Struchtrup [5]. Their closed system uses RO to separate saltwater into freshwater and a concentrated brine to store energy. To discharge this energy storage system, PRO is used to harness some of the energy of mixing from combining the brine and freshwater created in the RO stage. This combined stream is then added to the saltwater tank from which the RO stage draws. A schematic of this system can be seen in Fig. 2.2.

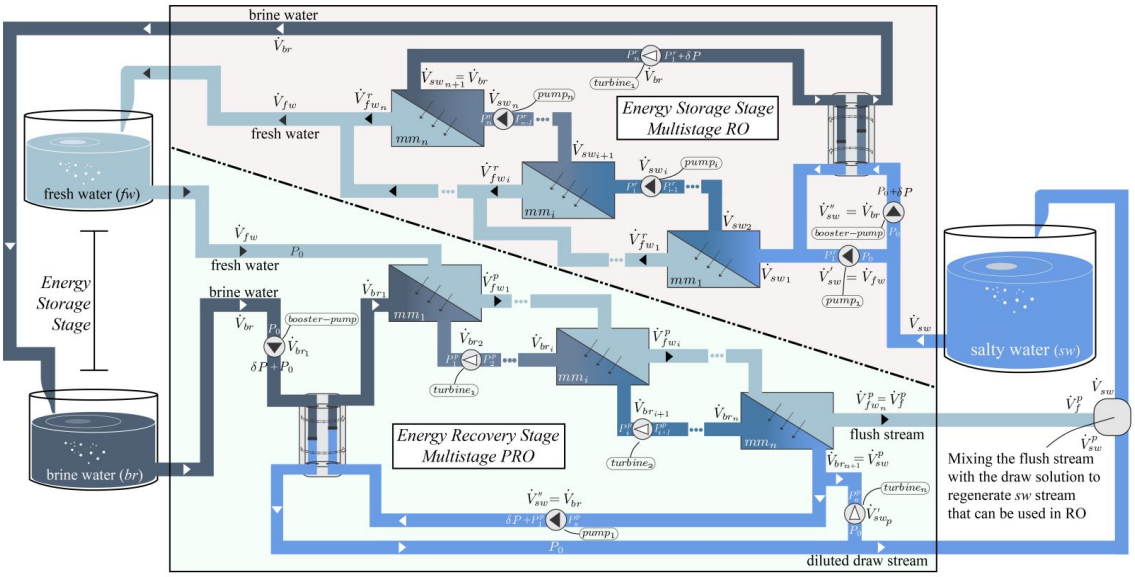

Figure 2.2: A conceptual OES system proposed by Bharadwaj & Struchtrup. (Reprinted from [5])

This system consists of well understood components: pumps, turbines, RO modules, PRO modules, tanks and pressure exchangers. Pressure exchangers are used to reduce energy lost in pumping and will be discussed in more detail in Chap. 5. Additionally, this system uses multistage RO and PRO to increase efficiency [5].

Bharadwaj & Struchtrup took a simplified, high level approach to modelling their OES system [5]. This is sufficient for a first look into the promise of the technology, but a more in-depth analysis is required to adequately analyze its potential. This report will outline the creation of a model to perform such an analysis.

There were two primary simplifications used by Bharadwaj & Struchtrup: ideal membranes and a membrane effectiveness factor [5]. Ideal membranes allow no salt to pass. This greatly increases the simplicity of the model, but salt leakage is a

significant source of entropy generation that cannot be ignored in a more in-depth analysis. Improving upon the model in this respect will help to show the significance of salt leakage on overall system efficiency.

The membrane effectiveness factor used was a simple way to model the RO and PRO membrane modules without having to dive into membrane transport equations, discretization and other significant sources of complexity. A perfect membrane module would have the difference in osmotic pressures of the exiting flows be equal to the hydraulic pressure difference. For exmaple, in PRO this means there would be no remaining power to be harnessed at the set hydraulic pressure. This was given a membrane effectiveness factor of 1. In reality, the exiting osmotic pressure differential is always higher than the hydraulic pressure differential for PRO. In RO, the exiting osmotic pressure differential will always be less than the hydraulic pressure differential. For realistic membrane modules, the membrane effectiveness factor will be less than one. For PRO, the membrane effectiveness factor, η_{mm}, is defined as [6]:

$$\eta_{mm} = \frac{\pi_{D,o} - \pi_{F,o}}{\pi_{D,o} - \Delta p}, \tag{2.2}$$

where the subscript D refers to the draw solution, F to the feed solution and o to the outlet flow as opposed to inlet flow.

For their work, Bharadwaj & Struchtrup used a membrane effectiveness factor of 0.9. This value is achievable, however it may reduce membrane power density [5]. The actual value of this factor depends greatly on the pressures, flow rates and concentrations of the fluid flows. Assuming a constant value is a great simplification, though quite useful for preliminary analysis.

With these simplifications, they were able to achieve round trip efficiencies of 50-60% at similar energy densities to a 500m pumped hydro plant [5]. This report seeks to build on this analysis and produce a more detailed model that can be used to evaluate a potential OES system. A single stage system will be focused on and many of the simplifying assumptions will be removed. This will decrease the round trip efficiencies of the system, the values of which will be crucial in determining if this technology is suitable for creation of a prototype.

Chapter 3

Theory

3.1 Membrane Transport Equations

To create a thermodynamically rigourous model of the PRO and RO necessary for an OES system, a model detailing how salt and water pass through the membranes is required. There are many membrane transport models that have been used, but by far the most prevalent today for RO and PRO is the solution-diffusion model [11]. In this model, the permeants dissolve into the membrane and then diffuse through it. Separation is achieved because the rates of dissolution and diffusion are different for different species (e.g., water and salt) [11]. The discussion that follows uses the solution-diffusion model as the method of membrane transport.

Membrane transport is driven by the non-equilibrium in chemical potential of solutions on either side of a membrane. The driving factors are the concentrations and the pressures of the solutions, as mentioned in Sec. 2.2.

Looking at a pure solvent on one side of a membrane with a solution on the other side, the molar chemical potential, $\bar{\mu}$, is [10]

$$\bar{\mu}_{ps}(T, p_{ps}) = \bar{g}_i(T, p_s) - \bar{\nu}_i(p_s - p_{ps}), \tag{3.1}$$

for the pure solvent and,

$$\bar{\mu}_s(T, p_s, X_i) = \bar{g}_i(T, p_s) + \bar{R}T\ln(\gamma_i X_i), \tag{3.2}$$

for the solution. $\bar{g}_i$ is the molar Gibbs free energy, p_s is the pressure of the solution, $\bar{\nu}_i$ is the molar volume, p_{ps} is the pressure of the pure solvent, $\bar{R}$ is the molar gas

constant, T is the temperature of the solution, γ_i is the activity coefficient of species i and X_i is the mole fraction of the solvent.

The difference between Eq. 3.2 and Eq. 3.1 for an infinitesimally small step is

$$d\bar{\mu}_i = \bar{R}Td\ln(\gamma_i X_i) + \bar{\nu}_i dp. \tag{3.3}$$

Since flux is driven by a gradient in chemical potential, we can define the flux, $\bar{J}_i$, as:

$$\bar{J}_i = -\bar{L}_i \frac{\partial \bar{\mu}_i}{\partial x}, \tag{3.4}$$

where $\bar{L}_i$ is a transport coefficient and not necessarily constant [11]. Using Eq. 3.3, Eq. 3.4 and the appropriate boundary conditions, Wijmans & Baker proceeded to develop the solution diffusion transport equations for RO [11]:

$$J^w = A(\Delta p - \Delta\pi), \tag{3.5}$$

$$J^s = B(C^{F,m} - C^{D,m}), \tag{3.6}$$

where J^w and J^s are the water and salt fluxes respectively, Δp is the differential pressure across the membrane, $\Delta\pi$ is the difference in osmotic pressure across the membrane, A and B are water and salt permeability of the membrane respectively, $C^{F,m}$ is the concentration of salt at the membrane on the feed side and $C^{D,m}$ is the concentration of the salt at the membrane on the draw side. Note that mass based values were used in Eq. 3.5 and Eq. 3.6 instead of the mole based values used in previous equations.

Additionally, Eq. 3.5 and Eq. 3.6 are for RO and need to be adjusted for use in PRO. For Eq. 3.5, the hydraulic and osmotic pressure terms are swapped to account for the reversed water flux in PRO. This maintains the standard of water flux, J^w, being positive. The draw and feed sides are also reversed in PRO, resulting in a high salinity draw solution and a low salinity feed solution. Therefore the concentration terms in Eq. 3.6 are swapped to account for this different definition and to keep the salt flux positive. The equations become, for PRO:

$$J^w = A(\Delta\pi - \Delta p), \tag{3.7}$$

$$J^s = B(C^{D,m} - C^{F,m}). \tag{3.8}$$

The osmotic pressure, π, is defined as [10]:

$$\pi = -\frac{\bar{R}T}{\bar{\nu}} \ln(\gamma_i X_i), \tag{3.9}$$

but is often used in a simplified form for dilute solutions [11]:

$$\pi = \frac{i\bar{R}T}{\bar{\nu}} X_j, \tag{3.10}$$

where X_j is the mole fraction of solute in the solution, $\bar{\nu}$ is the molar volume of the solution and assuming the activity coefficient is approximately one. i, the van't Hoff factor is a measure of how many particles a solute dissolves into. For the case of sodium chloride in water it has a value of 2. This linear relation between π and X_j allows for substitution of ratios of osmotic pressures for ratios of mole fractions or concentrations and can lead to great simplifications of the governing equations. However, care must be taken when using this approximation. The dilute solution approximation is invalid for high salinity solutions, such as those sometimes observed next to the membrane in RO and PRO.

3.2 Concentration Polarization

As can be seen in Eq. 3.6, salt flux has been defined as a function of the concentrations at the membrane interface. This is also true of the differential osmotic pressure in Eq. 3.5. This is an important distinction, because the concentration at the membrane interface can vary significantly from the concentration in the bulk solution. This is due to a phenomenon called concentration polarization (CP).

Note that throughout the remainder of this report, mass based quantities will be used unless mentioned otherwise. Molar based quantities are differentiated by the bar notation above the variable.

3.2.1 Concentration Polarization in RO

In RO, as water passes through the membrane preferentially to salt, salt builds up on the feed side of the membrane (saltwater side for RO) as seen in Fig. 3.1. This buildup of salt increases the concentration at the membrane and therefore the differential osmotic pressure across the membrane. This higher $\Delta\pi$ leads to lower water flux for

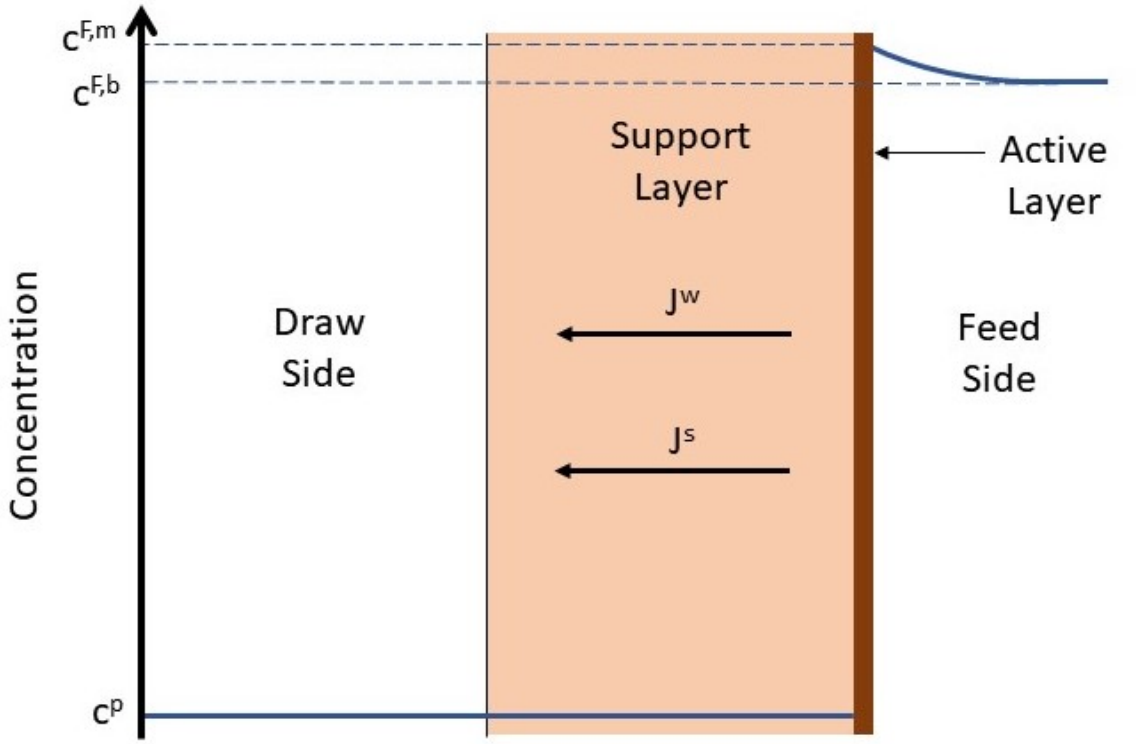

Figure 3.1: Concentration polarization in RO.

a given pressure differential. If CP is not accounted for, water flux will be significantly lower than expected [13].

An equation for concentration polarization can be derived from a mass balance of salt. Water is flowing towards the membrane bringing salt with it. A small amount of salt is passing through the membrane as defined in Eq. 3.6. Since there is a higher concentration of salt at the membrane, salt is diffusing away from the membrane towards the lower concentration bulk solution. Looking at the membrane on the feed side, there is a convective flux of salt, $J^w C$, and a diffusive flux of salt, $D_s \frac{dC}{dx}$. Note that in this case, $\frac{dC}{dx}$ will be negative. These two fluxes detail the flow of salt on the feed side. Some of the salt that comes in contact with membrane passes through. This is the salt flux through the membrane, J^s. A mass balance for the salt is created by putting this all together:

$$J^s = J^w C + D_s \frac{dC}{dx}, \tag{3.11}$$

where D_s is the salt diffusion coefficient and x is the perpendicular distance from

the membrane on the saltwater side. Integration can then be performed across the concentration polarization boundary layer, where the concentration is higher than that in the bulk solution:

$$\frac{C^{F,m} - \frac{J^s}{J^w}}{C^{F,b} - \frac{J^s}{J^w}} = \exp\left(J^w \delta / D_s\right), \tag{3.12}$$

where the superscript b refers to the bulk solution, m to the solution at the membrane and δ is the width of the boundary layer. However, since this width of the boundary layer isn't easily measurable, a mass transfer coefficient, k, is used instead. It also accounts for the diffusion coefficient and will be discussed further in Chap. 5. The equation now becomes:

$$\frac{C^{F,m} - \frac{J^s}{J^w}}{C^{F,b} - \frac{J^s}{J^w}} = \exp\left(J^w / k\right). \tag{3.13}$$

3.2.2 Concentration Polarization in PRO

In PRO, the water flux is in the opposite direction. Therefore, as shown in Fig. 3.2, the concentration on the draw side (saltwater side for PRO) is lower than the bulk solution. Since osmotic pressure is the driving force in PRO, as opposed to hydraulic pressure in RO, this decrease in concentration and corresponding decrease in differential osmotic pressure leads to decreased water flux [2].

An equation for this CP, referred to as external CP, can be derived in a similar manner to that shown above for RO. The only differences are that the water flux, J^w, is in the opposite direction and equation is for the draw side, rather than the feed side. Therefore the equation becomes:

$$\frac{C^{D,m} + \frac{J^s}{J^w}}{C^{D,b} + \frac{J^s}{J^w}} = \exp\left(-J^w / k\right). \tag{3.14}$$

In addition to external CP, in PRO there is also a significant decrease in water flux caused by internal CP. The majority of present day membranes chosen for their combination of high selectivity (low salt flux) and high water permeability are asymmetric. These membranes have a thin active layer on the high pressure side, with a relatively thicker support layer on the low pressure side to prevent mechanical failure of the membrane (Fig. 3.2). In PRO, since water is flowing from the low pressure side to the high pressure side, salt accumulates in this membrane support layer. If membranes were perfect (i.e., no salt flux) and there was pure water on the feed

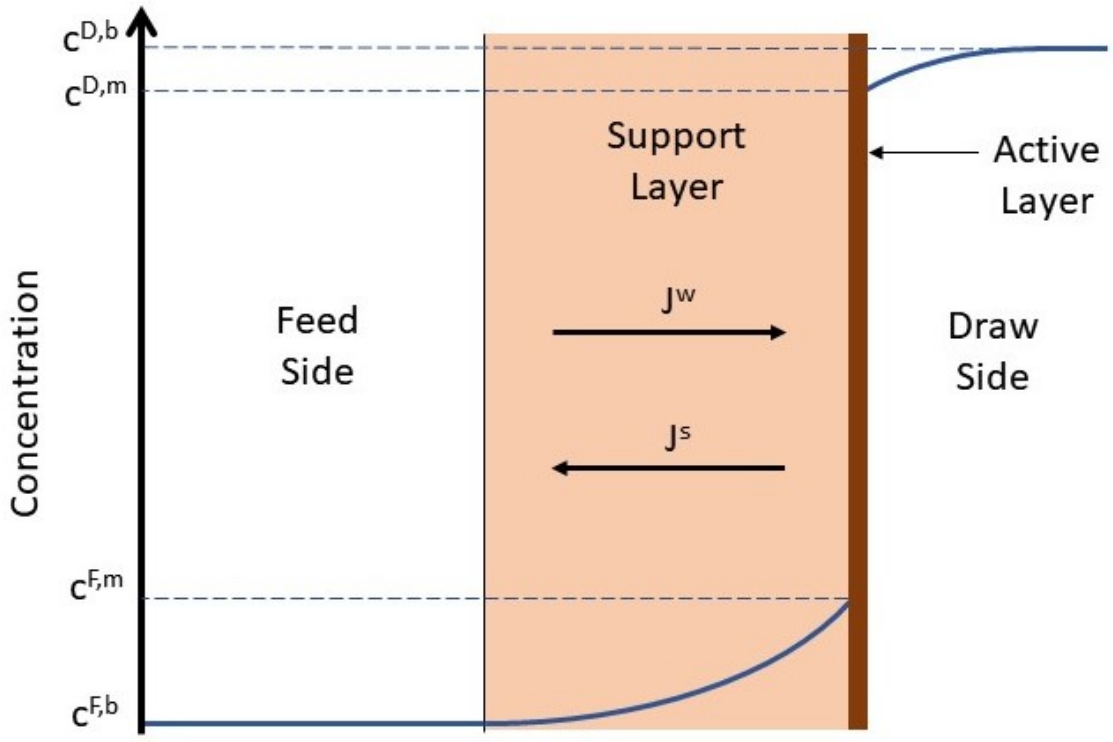

Figure 3.2: Concentration polarization in PRO.

(freshwater) side, this would not be an issue. However, since real membranes do have salt leakage, this accumulation of salt in the support layer increases the concentration at the membrane on the feed side. This decreases the differential osmotic pressure and therefore the flux [2].

Deriving internal CP begins similarly to external CP, however here the salt flux, J^s, is substituted from Eq. 3.8:

$$-B(C^{D,m} - C^{F,m}) = J^w C + \epsilon_m D_s \frac{dC}{dx}, \tag{3.15}$$

where ϵ_m is the porosity of the support layer which accounts for the reduced cross sectional area for diffusion in the support layer. The salt flux is also in the opposite direction relative to the convective and diffusive terms, when compared to Eq. 3.11. The equation can now be integrated and a second mass transfer coefficient, K, is introduced [13]:

$$\frac{C^{F,m}}{C^{D,m}} = \frac{B[\exp(J^w K) - 1] + J^w \frac{C^{F,b}}{C^{D,m}} \exp(J^w K)}{B[\exp(J^w K) - 1] + J^w}, \tag{3.16}$$

resulting in an implicit equation for the concentration of the draw solution at the membrane. K is a measure of the resistance to salt transport in the porous support layer and is calculated as [13]:

$$K = \frac{\tau t}{D_s \epsilon_m} = \frac{S}{D_s}, \tag{3.17}$$

where τ is the tortuosity, t is the thickness and S is the structure factor, all of the membrane's support layer. External CP on the feed (freshwater) side is neglected as the effects tend to be much less than that of internal CP [18].

External CP can be mitigated by enhanced mixing and increased flow along the membrane surface. Internal CP cannot be mitigated in this fashion. Instead, membranes with low salt leakage and thinner, less tortuous support layers are required. Internal CP is one of the primary limiting factors in having high power density per membrane area in PRO [4].

3.3 Ideal Work

The bottom up approach to modelling membrane transport detailed above serves as the foundation on which the OES model detailed in this report is built. However, it is also useful to have a benchmark against which to compare this OES system. While a lossless OES system would achieve a 100% efficiency as detailed in Sec. 2.3, it is also useful to look at how each stage, RO and PRO, performs. For RO this benchmark is the reversible work of separation, while for PRO it is the reversible work of mixing. These are identical for the RO and PRO stages when performing a full OES cycle, with just a sign change to indicate that work is required or produced.

The reversible work of mixing for ideal mixtures is calculated as [10]:

$$W_{mix}^{rev} = TS_{mix} = -T \sum_{\alpha} n_\alpha \bar{R} \ln X_\alpha, \tag{3.18}$$

where S_{mix} is the entropy of mixing, T is the temperature of the mixture and X_α is the mole fraction of species α in the mixture. W_{mix}^{rev} is the work that could be produced by beginning with all α pure substances and mixing them to create the mixture.

To determine the reversible work, W^{rev}, for either stage of an OES system, the difference of W_{mix}^{rev} from the beginning to the end of the process is calculated. For

example, for RO this becomes:

$$W_{RO}^{rev} = TS_{mix}^{fw} + TS_{mix}^{br} - TS_{mix}^{sw} < 0, \tag{3.19}$$

where S_{mix}^{fw} refers to the entropy of mixing for the solution in the freshwater tank and similarly for the other terms with the superscript br referring to the brine and sw to the initial saltwater. Note that this will be negative since RO requires work. PRO is the opposite process, so calculating the reversible work is identical to Eq. 3.19 with a reversal of signs resulting in positive work.

This reversible work can then be used to determine how efficiently each stage is performing. This efficiency is calculated for RO as:

$$\eta_{RO} = \frac{W_{RO}^{rev}}{W_{RO}}, \tag{3.20}$$

where W_{RO} is the actual work consumed by the RO stage. Similarly, efficiency for the PRO stage is

$$\eta_{PRO} = \frac{W_{PRO}}{W_{PRO}^{rev}}, \tag{3.21}$$

where W_{PRO} is the actual work produced by the PRO stage.

As mentioned above this is valid for ideal mixtures. In reality, saltwater is a non-ideal mixture, especially at higher concentrations. However, for the purpose of a benchmark to evaluate against, this approximation is acceptable. The added complexity of calculating the real reversible work of mixing is not necessary.

Chapter 4

System Design

The high level design of the OES system proposed in this report is very similar to that proposed by Bharadwaj & Struchtrup [5]. As discussed in Chap. 2, their system explored multistage RO and PRO. The system proposed in this report is simplified in using only single stage RO and PRO. However, this report will explore configurations for recirculating freshwater in the PRO stage that were not looked at in previous work.

4.1 RO Stage

The RO stage of the proposed OES system can be seen in Fig. 4.1. Saltwater is drawn from a tank, pressurized and run through the RO membrane module. The resulting freshwater stream then enters the freshwater tank. The brine stream, which is still at high pressure, is used to pressurize some of the incoming saltwater using a pressure exchanger (PX) before entering the brine tank. Since pressure exchangers require that both streams have equal flow rates, only a portion of the incoming saltwater stream can be pressurized with the PX. The remainder must be completely pressurized by a pump. Additionally, booster pumps are needed for the stream passing through the PX since there is a discrete pressure drop in the device. This configuration is identical to that proposed by Bharawadj & Struchtrup [5], with the exception of it being single stage, and the location of the booster pumps for the PX, which are arbitrary.

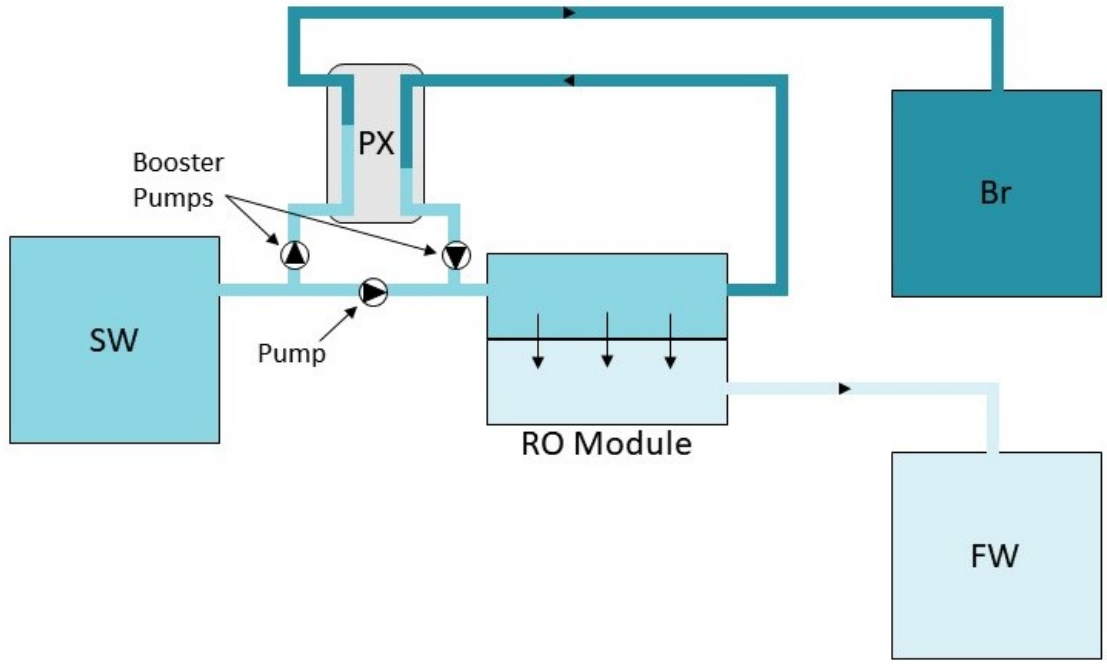

Figure 4.1: RO stage configuration for the proposed OES system.

4.2 PRO Stage

A proposed configuration of the PRO stage is shown in Fig. 4.2. Brine is drawn from the brine tank, pressurized in the PX and fed into the draw side of the PRO module. Freshwater is drawn from the freshwater tank and fed into the feed side of the PRO module. A small pump pressurizes the freshwater sufficiently to overcome any pressure losses within the piping and the module. The saltwater leaving the PRO module on the draw side is then split into two streams. One of equal flow rate to the incoming brine is run through the PX to pressurize the brine. As in the RO stage, booster pumps are required with the PX to overcome the pressure drop inherent in the device. The remaining saltwater is then run through a turbine, producing power. The streams are recombined and enter the saltwater tank. The stream leaving the freshwater side of the PRO module also flows into the saltwater tank. As with the RO stage, this PRO stage configuration is identical to that proposed by Bharadwaj & Struchtrup [5], with the exception of being single stage and the location of the PX booster pumps.

Adding the outgoing freshwater to the saltwater tank is a loss of potential work.

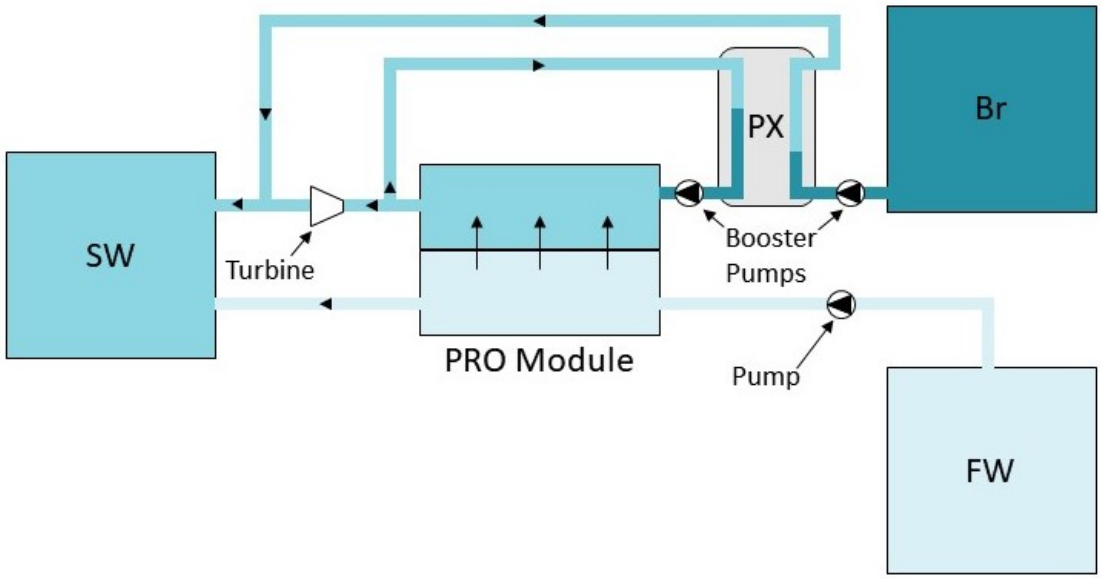

Figure 4.2: PRO stage configuration for the proposed OES system.

This freshwater could still be used as a feed solution in the PRO module, harnessing more of the energy of mixing. Therefore, an alternate PRO stage configuration is proposed, as shown in Fig. 4.3. This configuration is identical to the previous PRO configuration, but the freshwater is recirculated. The freshwater leaving the PRO module is returned to the freshwater tank instead of entering the saltwater tank. Due to salt leakage in the PRO module, this will lead to increased salinity in the freshwater tank, which will requiring periodic flushing.

4.3 Membrane Module

The key components in OES systems are the membrane modules. For the work in this report, the decision was made to use a single membrane module for both RO and PRO. This has the advantage of reducing the capital cost of the system. Unfortunately, it prevents the membrane module from being tailored to either RO or PRO specifically. This could be explored in future work as a method of increasing system efficiency.

Membrane modules come in a variety of configurations. One configuration is the spiral wound membrane module. These are created by layering membrane sheets with spacers. These layers are then wrapped around a central permeate collection tube, creating alternating channels for saltwater and freshwater. See Fig. 4.4 for reference.

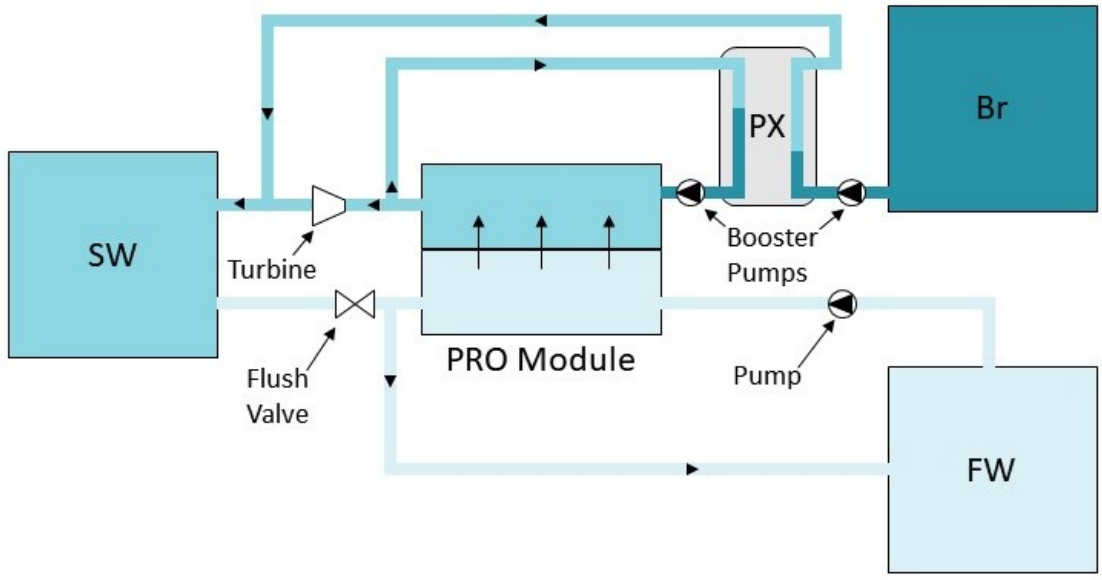

Figure 4.3: PRO stage configuration with freshwater recirculation for the proposed OES system.

The freshwater channels spiral towards the central tube where all the permeate is collected. Saltwater is fed into the module from one end and flows axially through the membrane channels and out the other end. Spiral wound membrane modules are the predominant type used in commercial RO [9].

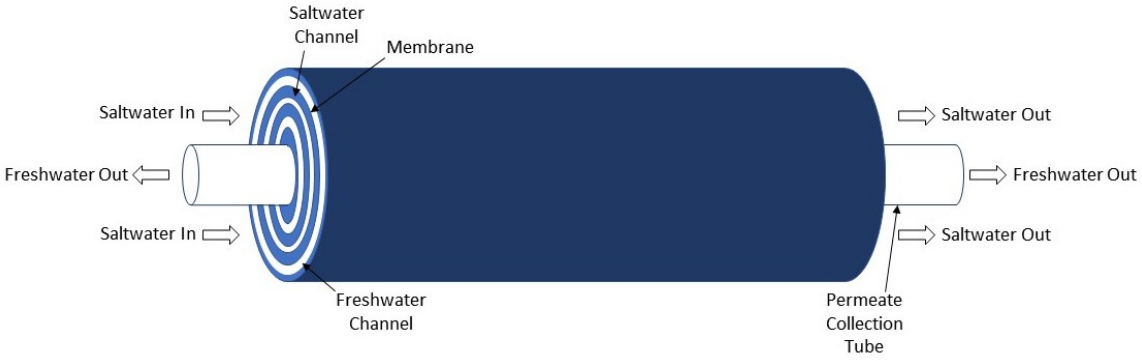

Figure 4.4: Spiral wound membrane module.

However, an alternate configuration appears to be more promising for PRO applications [21]. Membrane material is wrapped around to form small fibers. Thousands of these fibers are then put into a shell, as seen in Fig. 4.5. The ends of the shell are capped, with the hollow fibers passing through to the outside of the caps, allowing

for freshwater to be fed into one end, flowing out the other after passing through the shell. Saltwater is fed into a central perforated tube. It then flows radially through the shell filled with hollow fiber membranes. The saltwater then collects at the outer radius before flowing out of the module.

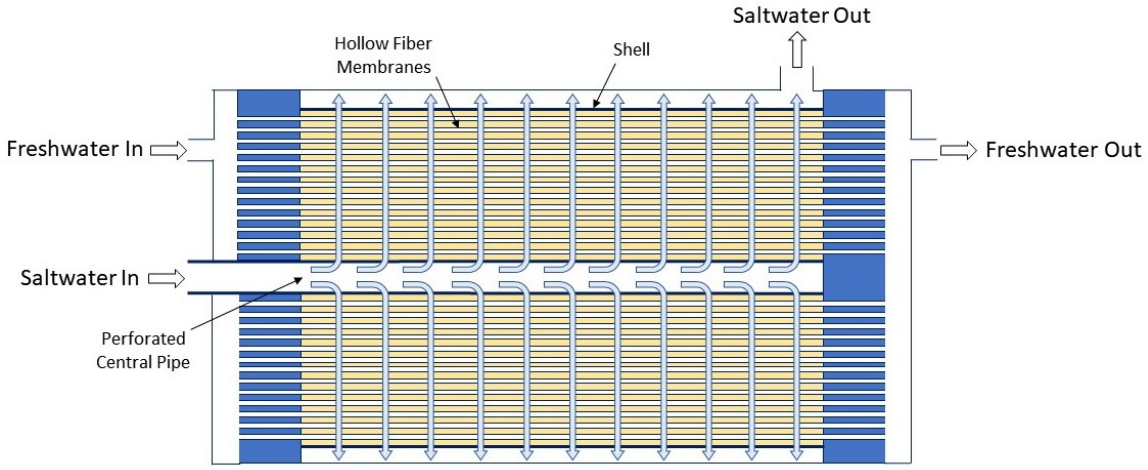

Figure 4.5: Hollow fiber membrane module cross section.

A hollow fiber membrane module was chosen for use in this work. This configuration typically allows for a higher pressure differential than spiral wound modules, increasing the range of potential operating conditions [21].

4.3.1 Membrane Module Parameters

With the choice of a HF membrane module, a module used by Shibuya et al. [17] was selected as the reference membrane module. This membrane module was, however, a 5-inch scale module. Therefore dimensions estimated from a schematic of a Toyobo HP5255SI-H3K membrane module were used for L_{mem}, R and R_c. These are the active module length, the active module radius and the radius of the perforated central tube respectively. Active module length refers to the length of the module in which the hollow fiber membranes are exposed to the shell side solution. Similarly with the active module radius.

The void fraction, ϵ, is the portion of the active volume in the shell which the saltwater solution will occupy, that free of hollow fibers. A void fraction of 0.5 was used as it is typical of values for this type of membrane module [3][14][17][25]. Together with the outer diameter of the hollow fibers, $d_{f,o}$, and the above noted physical mod-

ule parameters, ϵ was used to calculate the total active membrane area. See Chap. 5.

Parameter	Symbol	Value
Active module length	L_{mem}	0.682 m
Active module radius	R	0.0534 m
Central tube radius	R_c	0.0107 m
Void fraction	ϵ	0.5
Fiber outer diameter	$d_{f,o}$	1.8x10^{-4} m
Fiber inner diameter	$d_{f,i}$	9.4x10^{-5} m
Water permeability coefficient	A	7.4x10^{-13} m/s-Pa
Salt permeability coefficient	B	2.2x10^{-8} m/s
Structure factor	S	1.024x10^{-3} m
Diffusion coefficient	D_s	1.48x10^{-9} m^2/s
Temperature	T	298.15 K
Density of water	ρ_w	1000 kg/m^3
Dynamic viscosity of water	μ_w	8.9x10^{-4} Pa-s

Table 4.1: Model parameters [17].

Table 4.1 shows the membrane module parameters and some fluid properties used in this work. $d_{f,i}$ is the inner diameter of the hollow fibers. A, B and S are membrane parameters introduced in Chap. 3. The values of these four parameters and $d_{f,o}$ were all taken from Shibuya et al. [17].

The diffusion coefficient, D_s, was selected for typical conditions expected in the operation of the OES system [23]. T is the temperature at which the simulations were run. ρ_w and μ_w are the values used for the density and dynamic viscosity of pure water, respectively. These parameters are all used in various calculations in the OES system model.

Chapter 5

Modelling

With the underlying equations detailed in Chap. 3 and the design outlined in Chap. 4, the creation of the models can now be examined. The OES model was created by first making models for the individual components (PRO module, RO module, pumps, turbines and pressure exchangers) and then assembling the overall OES model by putting these component models together.

Throughout these models, functions are used to calculate the density, viscosity and osmotic pressure of saltwater. These functions are based on work done by researchers at MIT and modified or created by Pani Energy Inc. before being provided for use in this work. The viscosity and density functions are based on equations by Sharqawy et al. [16]. The osmotic pressure function is based on equations by Nayar et al. [12]. These functions take salinity, temperature and, in the case of the density, pressure as inputs.

Note that in Chap. 3 the subscripts F and D were used to refer to the feed and draw solutions. For PRO the feed solution is inside the fibers and the draw solution is in the shell. On the other hand, for RO the feed solution is in the shell and the draw solution is inside the fibers. For that reason, the below equations use the subscripts f and sh to refer to the fiber and shell sides. This avoids confusion when looking at the pressure drop equations as the same subscript can now refer to both processes.

5.1 PRO Model

The key components in an OES system are the membrane modules. The PRO and RO module models are very similar, with the key difference being the direction of the

water flux across the membrane.

Note that the membrane module models detailed here ignore transient conditions (e.g., startup) and are created based on equations that assume steady state operation. This decision was reinforced by comments from Pani Energy Inc. and work by Palacin [9]. They both noted that steady state was achieved fairly quickly, on the order of one minute or less, while a charge or discharge cycle is typically expected to last much longer for an OES system in operation.

5.1.1 Discretization

As discussed in Sec. 4.3, a hollow fiber membrane module will be used for both PRO and RO. In these modules, the freshwater within the hollow fibres flows axially. The high salinity fluid enters the module via a perforated central pipe. There are no hollow fibers within this pipe and the pressure drop is minimal, so the high salinity fluid can be modelled as being supplied at the central pipe, and only flowing in the radial direction within the module. Similarly, the fluid is collected at the outer radius of the module and flows out of the module from this point with minimal change in pressure or salinity. A cross section of a hollow fiber membrane module is shown in Fig. 5.1. The size of the hollow fibers and the space between them are greatly exaggerated.

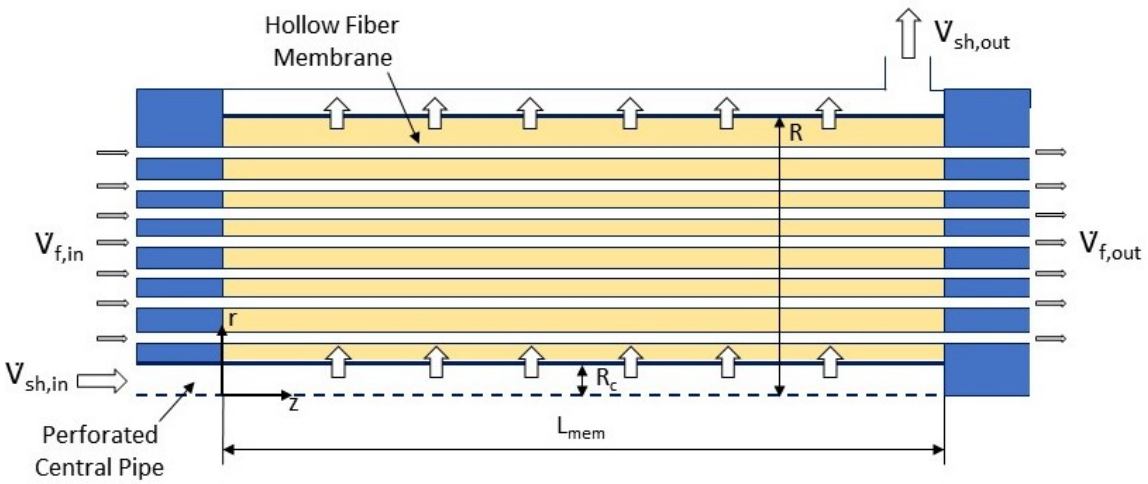

Figure 5.1: Cross section of a hollow fiber membrane module.

Since there is axial flow of the freshwater and radial flow of the high salinity water, this results in a two dimensional model. Radial symmetry is used to prevent

the model from becoming three dimensional.

To model the changing conditions in the axial (z) and radial (r) directions, the module must be discretized into N_z axial divisions and N_r radial divisions. The axial length of the cells, Δz, is calculated:

$$\Delta z = \frac{L_{mem}}{N_z}. \tag{5.1}$$

Recall that L_{mem} is the active length of the membrane module, the length where the hollow fibres are exposed to the shell side solution. Similarly, the radial length of the cells, Δr, is found with the following equation:

$$\Delta r = \frac{R - R_c}{N_r}, \tag{5.2}$$

where R is the module's active radius and R_c is the radius of the central tube. A constant radial length was chosen, meaning the cells will have larger volume towards the outside of the module. This will be accounted for in the following calculations.

A visual representation of this discretization is shown in Fig. 5.2. This image shows a 3x3 discretization, with coordinates noted in the lower left and upper right corners. $\dot{m}_b$ represents the mass flows in the bulk solution, J the fluxes and C_m the concentrations at the membranes, all for both salt and water. This notation with symbols representing multiple variables was used to decrease complexity of the figure. P represents the pressure in a given cell. The subscript f refers to the fiber side and sh to the shell side. $P_{f,in}$, $P_{sh,in}$, $P_{f,out}$ and $P_{sh,out}$ are the pressure boundary conditions. The subscript in refers to the parameter at the inlet to the module while out refers to the outlet. All of these variables will be discussed further throughout the remainder of this section. Fig. 5.2 shows at which points in the cells each value is calculated. The subscripts in the below equations will indicate this as well.

5.1.2 Membrane Area

The hollow fibers in this type of membrane modules are typically cross-wound, spiralling at a given radius as they proceed through the module. This leads to different fiber length depending on the radius at which the fiber is located. For this model, the hollow fibers were assumed to be straight and regularly spaced throughout the active portion of the module.

$A_{m,T}$ is the total active membrane area in the module. It is related to the void

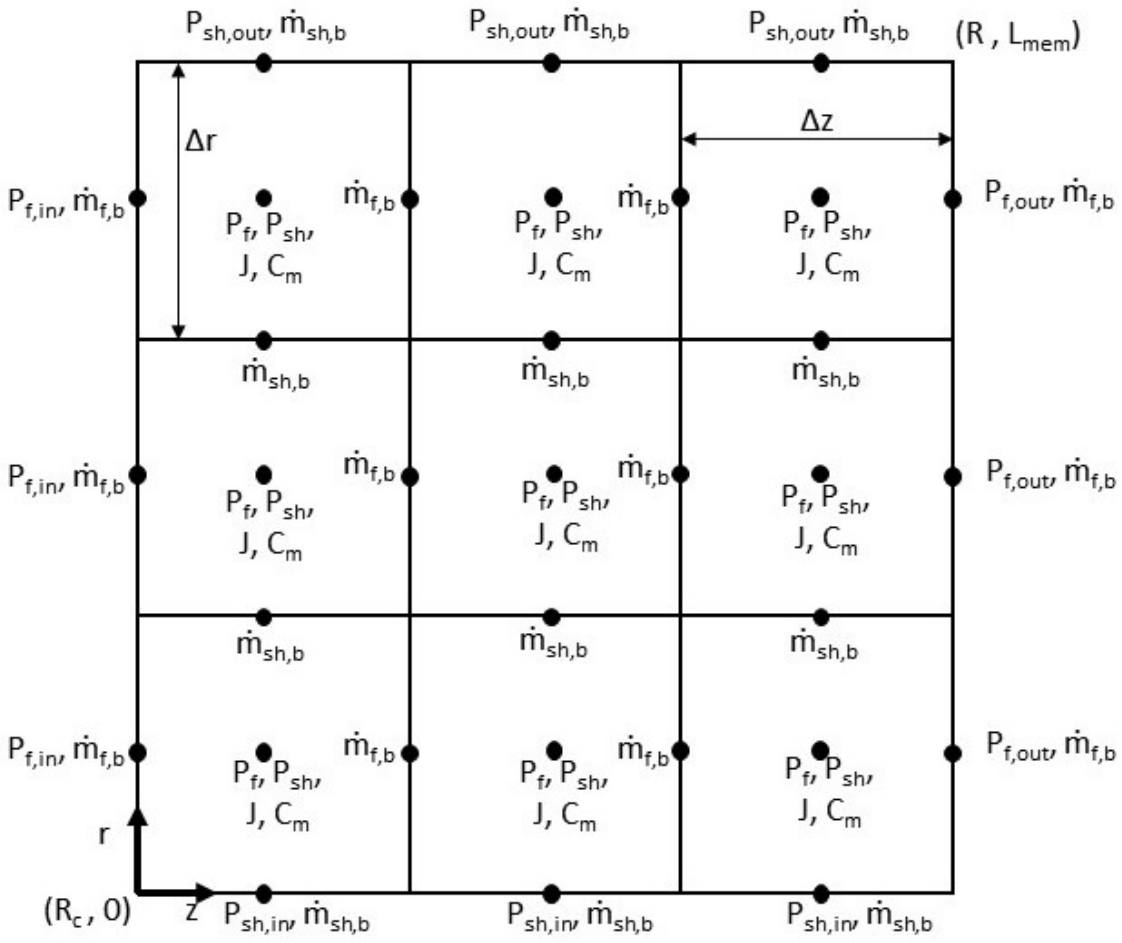

Figure 5.2: Cross section showing a representation of a 3x3 discretization of the hollow fiber membrane module.

fraction, ϵ, as:

$$\epsilon = 1 - \left[\frac{A_{m,T} d_{f,o} / 4 L_{mem}}{\pi (R^2 - R_c^2)} \right]. \tag{5.3}$$

With this equation, two of R, R_c and ϵ are required as inputs to the model, depending on the information available. $A_{m,T}$ is typically provided.

The active membrane area per unit volume, A_m, is important for calculations since the cell volume changes with radius. It is calculated as:

$$A_m = \frac{A_{m,T}}{\pi (R^2 - R_c^2) L_{mem}}. \tag{5.4}$$

Another value sometimes listed when describing a membrane module is the total number of fibres in the module, n. With the straight fiber approximation, this

becomes:

$$n = \frac{A_{m,T}}{\pi d_{f,o} L_{mem}} = \frac{A_m}{d_{f,o}}(R^2 - R_c^2), \tag{5.5}$$

and the number of fibres per cell, n_c, is

$$n_c = n\frac{(r+\Delta r)^2 - r^2}{R^2 - R_c^2} = \frac{A_m}{d_{f,o}}((r+\Delta r)^2 - r^2), \tag{5.6}$$

where r is the inner radius of the cell in question.

5.1.3 Mass Balances

With the equations detailing the physical membrane module, the fluid flow and mass transport can now be described. The first of these are the mass balances of salt and water within the cells in the shell and the hollow fibers. Discrete balances are presented as required for numerical methods.

The mass balance of water in hollow fibers is

$$\dot{m}^{w,f}_{z+\frac{\Delta z}{2},r} = \dot{m}^{w,f}_{z-\frac{\Delta z}{2},r} - \rho_w J^w_{z,r} A_m \pi((r+\Delta r)^2 - r^2)\Delta z, \tag{5.7}$$

where ρ_w is the density of pure water, $\dot{m}^{w,f}_{z-\frac{\Delta z}{2},r}$ is the mass flow rate of water in the fiber entering the cell at coordinates z, r while $\dot{m}^{w,f}_{z+\frac{\Delta z}{2},r}$ is exiting the cell. $J^w_{z,r}$ is the volume flux of water per area of membrane, defined as positive passing from the hollow fibres (freshwater side) to the shell (saltwater side) for PRO.

Similarly, the mass balance of water in the shell is

$$\dot{m}^{w,sh}_{z,r+\frac{\Delta r}{2}} = \dot{m}^{w,sh}_{z,r-\frac{\Delta r}{2}} + \rho_w J^w_{z,r} A_m \pi((r+\Delta r)^2 + r^2)\Delta z, \tag{5.8}$$

where $\dot{m}^{w,sh}_{z,r+\frac{\Delta r}{2}}$ is the mass flow rate of water in the shell exiting the cell in the radial direction.

The mass balance of salt in hollow fibre is

$$\dot{m}^{s,f}_{z+\frac{\Delta z}{2},r} = \dot{m}^{s,f}_{z-\frac{\Delta z}{2},r} + J^s_{z,r} A_m \pi((r+\Delta r)^2 + r^2)\Delta z, \tag{5.9}$$

where $\dot{m}^{s,f}_{z-\frac{\Delta z}{2},r}$ is the fiber side mass flow rate of salt and $J^s_{z,r}$ is the mass flux of salt per area of membrane, defined as positive passing from the shell to the hollow fibres.

The mass balance of salt in the shell is

$$\dot{m}^{s,sh}_{z,r+\frac{\Delta r}{2}} = \dot{m}^{s,sh}_{z,r-\frac{\Delta r}{2}} - J^{s}_{z,r} A_m \pi((r+\Delta r)^2 + r^2)\Delta z. \tag{5.10}$$

5.1.4 Flow Rates

From the mass flow rates of water and salt, the volumetric flow rate, $\dot{V}$, is

$$\dot{V} = \frac{\dot{m}^w + \dot{m}^s}{\rho}, \tag{5.11}$$

where ρ is the density of the solution. The density of the solution can be computed from the salinity of the solution, s, using the functions described at the beginning of the chapter. The salinity is defined as:

$$s = \frac{\dot{m}^s}{\dot{m}^w + \dot{m}^s}. \tag{5.12}$$

5.1.5 Pressure Drops

As the fluids pass through the module, the pressures decrease due to hydraulic losses. Since pressure differential is a key component of water flux, as shown in Eq. 3.5, these pressure changes will affect the composition and flow rates of the outgoing fluids.

The pressure drop in the shell side is described by the Ergun equation [8]:

$$\frac{\partial p^{sh}}{\partial r} = \left[\frac{150(1-\epsilon)^2 \mu^{sh} v^{sh}}{\epsilon^3 (1.5 d_{f,o})^2} + \frac{1.75(1-\epsilon)\rho (v^{sh})^2}{\epsilon^3 (1.5 d_{f,o})}\right], \tag{5.13}$$

where μ^{sh} is the dynamic viscosity of the fluid in the shell and v^{sh} is the superficial velocity, the velocity the fluid would have if there were no hollow fibres. This velocity is defined as:

$$v^{sh} = \frac{\dot{V}^{sh}}{2\pi r \Delta z}. \tag{5.14}$$

The pressure drop in the fibers is described by the Hagen-Poiseuille equation [17]:

$$\frac{\partial p^f}{\partial z} = -\frac{128 \mu \frac{\dot{V}^f}{n_c}}{\pi d^4_{f,i}}, \tag{5.15}$$

where μ^f is the dynamic viscosity of the fluid in the fiber.

For the case of the intermediate pressures, these equations are simply discretized.

For the shell side it becomes:

$$p^{sh}_{z,r+\Delta r} = p^{sh}_{z,r} - \left[\frac{150(1-\epsilon)^2\mu^{sh}_{z,r}v^{sh}_{z,r}}{\epsilon^3(1.5d_{f,o})^2} + \frac{1.75(1-\epsilon)\rho_{z,r}(v^{sh}_{z,r})^2}{\epsilon^3(1.5d_{f,o})}\right]\Delta r. \tag{5.16}$$

Similarly, the fiber side pressure drop over a cell becomes:

$$p^{f}_{z+\Delta z,r} = p^{f}_{z,r} - \frac{128\mu^{f}_{z,r}\dot{V}^{f}_{z,r}d_{f,o}}{\pi d^4_{f,i}A_m((r+\Delta r)^2 - r^2)}\Delta z. \tag{5.17}$$

These are second order approximations of central differentials. However, for the pressure drop from the inlet pressures to the first cells and from the last cells to the outlet pressures, only forward and backwards differentials can be used. Additionally, there is only a half step between these pressures, $\frac{\Delta z}{2}$ and $\frac{\Delta r}{2}$ for the fiber and shell side pressures respectively. Therefore Taylor series were used to expand these pressure drops and thus create a second order approximation. Refer to Fig. 5.2 for a visual depiction of where all of the variables are calculated for each cell.

With these calculations, the shell side inlet pressure, $P_{sh,in}$, is used to find the shell side pressure in the first radial cell, $p^{sh}_{z,\frac{\Delta r}{2}}$, as:

$$9p^{sh}_{z,\frac{\Delta r}{2}} = 8P_{sh,in} + p^{sh}_{z,\frac{3\Delta r}{2}} - \left[\frac{150(1-\epsilon)^2\mu^{sh}_{z,R_c}v^{sh}_{z,R_c}}{\epsilon^3(1.5d_{f,o})^2} + \frac{1.75(1-\epsilon)\rho_{z,R_c}(v^{sh}_{z,R_c})^2}{\epsilon^3(1.5d_{f,o})}\right]3\Delta r, \tag{5.18}$$

where the subscript z, R_c refers to the value being calculated using the mass flow rates at $r = R_c$ and z.

The fiber side inlet pressure, $P_{f,in}$, is used to find the fiber side pressure in the first axial cell, $p^{f}_{\frac{\Delta z}{2},r}$, as:

$$9p^{f}_{\frac{\Delta z}{2},r} = 8P_{f,in} + p^{f}_{\frac{3\Delta z}{2},r} - \frac{128\mu^{f}_{0,r}\dot{V}^{f}_{0,r}d_{f,o}}{\pi d^4_{f,i}A_m((r+\Delta r)^2 - r^2)}3\Delta z, \tag{5.19}$$

where the subscript $0, r$ refers to the value being calculated using the mass flow rates at $z = 0$ and r.

Similar methods were used to calculate the pressures in the last axial cell on the fiber side and the last radial cell on the shell side.

5.1.6 Membrane Transport

With the fluid flow taken care of, the only thing remaining is the transport of water and salt across the membrane. The equations shown here are the discretized form of those introduced in Chap. 3. The water flux becomes:

$$J^w_{z,r} = A[(\pi^{sh,m}_{z,r} - \pi^{f,m}_{z,r}) - (p^{sh}_{z,r} - p^f_{z,r})], \tag{5.20}$$

and salt flux is

$$J^s_{z,r} = B(C^{sh,m}_{z,r} - C^{f,m}_{z,r}), \tag{5.21}$$

where $C^{f,m}_{z,r}$ is the concentration of salt at the membrane on the fiber side and $C^{sh,m}_{z,r}$ is the concentration of salt at the membrane on the shell side. These are mass concentrations, the mass of salt per volume of solution, and are related to salinity by:

$$s = \frac{C}{\rho}, \tag{5.22}$$

where ρ is the density of the solution.

Internal concentration polarization becomes:

$$\frac{C^{f,m}_{z,r}}{C^{sh,m}_{z,r}} = \frac{B[\exp(J^w_{z,r}K) - 1] + J^w_{z,r}\frac{C^{f,b}_{z,r}}{C^{sh,m}_{z,r}}\exp(J^w_{z,r}K)}{B[\exp(J^w_{z,r}K) - 1] + J^w_{z,r}}. \tag{5.23}$$

Note that for a given cell, the bulk concentrations are calculated using the average of the mass flows of salt and water entering and exiting the cell. That is, $C^{f,b}_{z,r}$ is a function of the average of $\dot{m}^{w,f}_{z-\frac{\Delta z}{2},r}$ and $\dot{m}^{w,f}_{z+\frac{\Delta z}{2},r}$, and the average of $\dot{m}^{s,f}_{z-\frac{\Delta z}{2},r}$ and $\dot{m}^{s,f}_{z+\frac{\Delta z}{2},r}$.

For external concentration polarization on the shell side, the ratio of concentrations are:

$$\frac{C^{sh,m}_{z,r} + \frac{J^s_{z,r}}{J^w_{z,r}}}{C^{sh,b}_{z,r} + \frac{J^s_{z,r}}{J^w_{z,r}}} = \exp(-J^w_{z,r}/k_{z,r}), \tag{5.24}$$

where k is

$$k = \frac{ShD_s}{d_{f,o}}, \tag{5.25}$$

and the Sherwood number is calculated as [25]:

$$Sh = 0.45Re^{0.1}Sc^{1/3}. \tag{5.26}$$

Here, Re is the Reynold's number and Sc is the Schmidt number. Note that there are many empirical equations for the Sherwood number. They depend on the module configuration, solution composition as well as the flow rates and pressures. The equation used here is for a module being used for PRO that is very similar to the module the membrane parameters in Sec. 4.3 were based off of. The equation was empirically found by Tanaka et al. [25].

The Reynold's number is defined as:

$$Re = \frac{d_{f,o} u^{sh} \rho}{\mu^{sh}}, \tag{5.27}$$

where u^{sh} is the flow velocity in the shell:

$$u^{sh} = v^{sh} \epsilon. \tag{5.28}$$

The Schmidt number is

$$Sc = \frac{\mu^{sh}}{\rho D_s}. \tag{5.29}$$

5.1.7 Model Architecture

With the above equations, a MATLAB model was created to simulate the operation of a hollow fibre PRO module. A function was used to create a system of equations comprising of the above equations for each cell in the discretized module.

MATLAB's *lsqnonlin* function was then used to solve this system of equations. This function solves nonlinear least squares problems, which is how the system of equations is set up. MATLAB's *fsolve* function, which solves systems of nonlinear equations, was also used in early versions of the model. Both functions produced the same results, however *lsqnonlin* complete the optimization faster.

The boundary conditions input to the model are the shell side pressure into and out of the module, the fiber side pressure into the module, the shell and fiber side salinities into the module, and the temperature of the module. All pressures are gauge pressures, relative to the fiber side outlet pressure which therefore was set at 0. The model outputs the total mass flow rates of fluid into and out of the module on both the fiber and shell sides, as well as the salinities of the out-flowing fluid on each side.

The inlet and outlet pressures were used as inputs to the model rather than some combination of pressures and mass flow rates. Inputting flow rates would require

conditions to limit the mass flow rates to positive values. *lsqnonlin* does allow bounds to be put on variables, but when the mass flow rates were constrained this led to issues converging on a solution.

5.1.8 Model Verification

Once the PRO module model was created, it was verified using experimental data collected by Tanaka et al. [25]. Their research was chosen as they used a membrane module with similar characteristics to that selected for use in the OES system presented in this report. The module parameters and operating conditions can be seen in Table 5.1. Note that the precise active length and radii of the module were not noted in their paper. The length was calculated by using the number of fibers in the module, the total membrane area and the outer diameter of the fibers as inputs to Eq. 5.5. The radius of the central tube was set at 10.7 cm, the outer radius of a standard 1/2" pipe. This dimension was indicated in a schematic of a Toyobo HP5255SI-H3K membrane module. Along with the void fraction, this was used as an input to Eq. 5.3 to calculate the active module radius, R. Additionally, Tanaka et al. accounted for the cross-winding [25] which, as mentioned above, was not done in this report.

Parameter	Symbol	Value
Void fraction	ϵ	0.458
Total number of fibers	n	220 000
Total membrane area	$A_{m,T}$	70.5 m^2
Fiber outer diameter	$d_{f,o}$	1.75x10^{-4} m
Fiber inner diameter	$d_{f,i}$	8.5x10^{-5} m
Water permeability coefficient	A	7.5x10^{-13} m/s-Pa
Salt permeability coefficient	B	9.72x10^{-9} m/s
Structure factor	S	1.024x10^{-3} m
Fiber side inlet molar concentration	$\bar{C}_{f,i}$	0 mol/L
Shell side inlet molar concentration	$\bar{C}_{sh,i}$	1 mol/L

Table 5.1: PRO verification parameters [25].

Fig. 5.3 shows the average flux, J_{ave}, in the membrane module. This is the total flux divided by the total active membrane area of the module. The figure compares the experimental and simulated results from Tanaka et al. [25] to the simulated results from the model presented in this report. The results shown are for an inlet flowrate of 8 lpm for both the freshwater and the high salinity water. Additional results can be seen in Appendix A for different operating conditions.

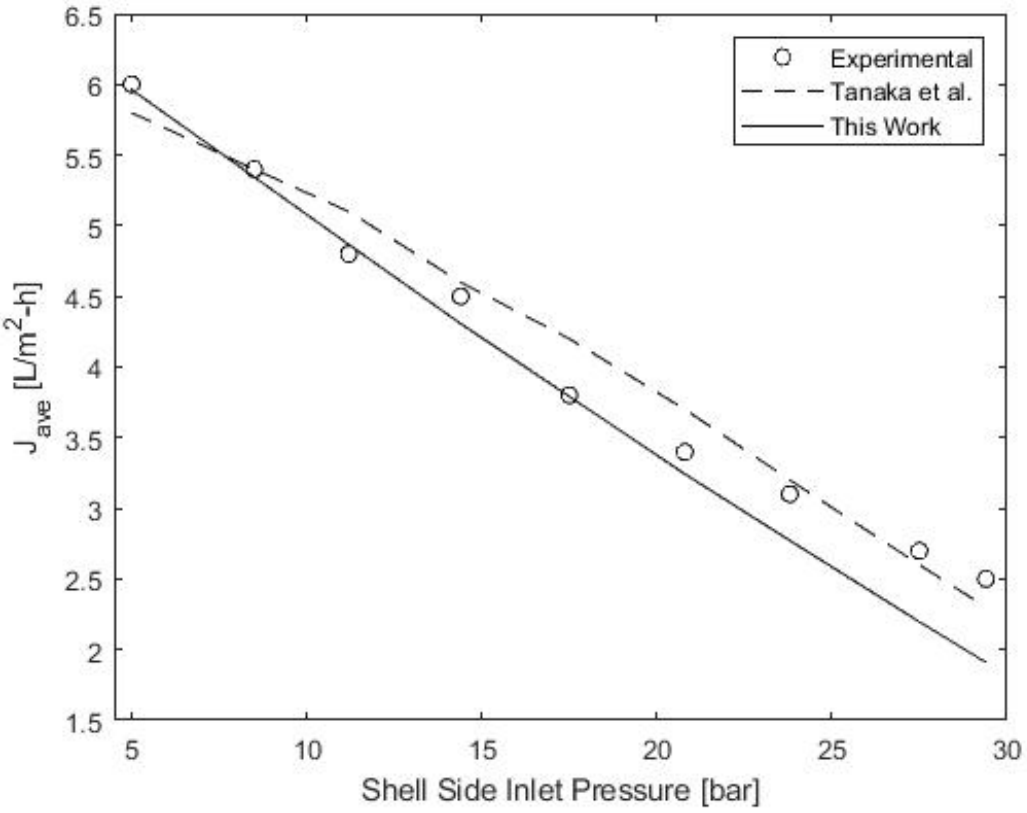

Figure 5.3: Results from the PRO module model presented in this report compared to experimental and simulated results by Tanaka et al. [25]. Data is for entering flowrates of 8 lpm for both freshwater and high salinity water.

As can be seen in Fig. 5.3, the proposed model generally agrees quite well with the data, although it tends to deviate at higher shell side pressures. The error varies between 0.2% and 24.1% for this model and is calculated as:

$$e_{PRO} = \frac{J_{ave}^{mod} - J_{ave}^{exp}}{J_{ave}^{exp}}, \tag{5.30}$$

where J_{ave}^{exp} is the average flux from the experimental data and J_{ave}^{mod} is that of the model. The model proposed by Tanaka et al. [25] produced errors varying from 0% to 10.5%. The error achieved by the proposed model is a good starting point to give an idea of the promise of an OES system.

5.1.9 Future Work

As can be seen from the larger errors at some operating conditions, improvements can be made to this PRO module model. One such improvement is accounting for cross-winding of the fibers. This would make the fiber length a function of radius, increasing the complexity of some calculations such as that for A_m and the pressure drop in the fibers.

Additionally, A, B and S could be refined. These coefficients are all found by fitting models to experimental results. Since the models used to determine these coefficients are slightly different than the model presented here, this would lead to different results. These values are also assumed to be constant in the creation of this model. However, these parameters have been shown to be dependent on concentration and/or pressure [22][7].

Another value that has been assumed constant is the diffusion coefficient, D_s. However it is also dependant on concentration [23]. Changing the diffusion coefficient will impact the affects of concentration polarization and therefore water and salt flux.

Finally, this model is based on steady state equations. This is an assumption that is used in most PRO models, however in the case of an OES system it is not fully accurate. A transient model for RO was explored by Palacin in his 2014 thesis [9]. He does this by coupling a macroscopic model, such as the solution-diffusion model used here, with a microscopic model. However, creating a transient model is a significant amount of work and adds considerable complexity to the model. At this point in the development of this type of OES system it is likely not necessary as steady state operation is generally expected. However, for the configuration with freshwater recirculation a transient model could add insight as operating parameters and system design are fine tuned.

5.2 RO Model

The RO module model is created in the same manner as the PRO model with the same underlying assumptions. Since the same membrane module is being used, the discretization and physical parameters such as membrane area calculations are identical.

The first key difference is the direction of water flux. In PRO water flows from the fiber side to the shell side. In RO it flows in the opposite direction. Therefore,

for the RO module model, water flux, J^w, is defined as positive flowing from the shell to the fiber. This affects the mass balances of water which are adjusted from Eq. 5.7 and Eq. 5.8 to become:

$$\dot{m}^{w,f}_{z+\frac{\Delta z}{2},r} = \dot{m}^{w,f}_{z-\frac{\Delta z}{2},r} + \rho_w J^w_{z,r} A_m \pi((r+\Delta r)^2 - r^2)\Delta z, \tag{5.31}$$

$$\dot{m}^{w,sh}_{z,r+\frac{\Delta r}{2}} = \dot{m}^{w,sh}_{z,r-\frac{\Delta r}{2}} - \rho_w J^w_{z,r} A_m \pi((r+\Delta r)^2 + r^2)\Delta z. \tag{5.32}$$

Additionally, there is no incoming freshwater stream to the module, only saltwater. Therefore alternate equations are needed for the fiber side water and salt mass flow rates exiting the first axial cells:

$$\dot{m}^{w,f}_{\Delta z,r} = \rho_w J^w_{\frac{\Delta z}{2},r} A_m \pi((r+\Delta r)^2 - r^2)\Delta z, \tag{5.33}$$

$$\dot{m}^{s,f}_{\Delta z,r} = J^s_{\frac{\Delta z}{2},r} A_m \pi((r+\Delta r)^2 + r^2)\Delta z. \tag{5.34}$$

In reverse osmosis, both water and salt flux are in the same direction. They pass through the active layer of the membrane and then through the porous support layer to the fiber side as seen in Fig. 3.1. Since these flows are both in the same direction, flowing from the active layer out through the support layer and into the bulk fiber side solution, the active layer of the membrane never interacts with this bulk solution during steady state operation. Instead the active layer only interacts with the water and salt that has just passed through the membrane on the fiber side. This solution of water and salt that has passed through the membrane is called permeate. The concentration of this permeate, C^p, is the relevant factor for water and salt flux. Eq. 5.20 and Eq. 5.21 now become:

$$J^w_{z,r} = A[(p^{sh}_{z,r} - p^f_{z,r}) - (\pi^{sh,m}_{z,r} - \pi^p_{z,r})], \tag{5.35}$$

$$J^s_{z,r} = B(C^{sh,m}_{z,r} - C^p_{z,r}), \tag{5.36}$$

where $\pi^p_{z,r}$ is the osmotic pressure of the permeate. Note that the equation for J^w has been adjusted to account for the new definition of positive water flux flowing from the shell side to the fiber side. The permeate concentration is calculated as:

$$C^p = \frac{\rho J^s}{(J^s + \rho_w J^w)}, \tag{5.37}$$

where ρ is the density of the permeate solution.

The equation for external concentration polarization, Eq. 3.13, is written as follows in discretized form:

$$\frac{C_{z,r}^{sh,m} - \frac{J_{z,r}^{s}}{J_{z,r}^{w}}}{C_{z,r}^{sh,b} - \frac{J_{z,r}^{s}}{J_{z,r}^{w}}} = \exp(J_{z,r}^{w}/k_{z,r}). \tag{5.38}$$

There is no internal concentration polarization in RO.

The last adjustment from the PRO model is using a revised equation for the Sherwood number. Since the water flux is in the opposite direction, the flow characteristics that affect external concentration polarization are different in RO. The equation used is from a paper by Sekino [15] for reverse osmosis using a hollow fiber membrane module. This equation for the Sherwood number is [15]

$$Sh = 0.048 Re^{0.6} Sc^{1/3}. \tag{5.39}$$

The remaining equations such as those for pressure drop are identical to those used in the PRO module model and can be seen in Sec. 5.1. Additionally, the MATLAB model was created using the same methods: creating system of equations and then solving it with MATLAB's *lsqnonlin* function. There is no incoming freshwater flow for this RO module, so the inputs and outputs related to this flow in PRO were not included for the RO module model.

5.2.1 Model Verification

As with the PRO module model, the RO model was also verified using experimental data. This experimental data was collected by Sekino [15]. Note that the data was not explicitly listed in the paper cited, so values were estimated from plots. The module parameters and operating conditions for the verification can be seen in Table 5.2. Sekino accounted for cross-winding [15] which was not done in this report.

Fig. 5.4 shows the ratio of concentrations between the produced freshwater and the incoming saltwater. Fig. 5.5 shows the flow rate of freshwater produced. These figures compare the experimental results from Sekino [15] to the simulated results from the model presented in this report.

As can be seen in Fig. 5.4 and Fig. 5.5, the proposed model does deviate significantly from the experimental results at high recovery ratios. However, the general trend of the results is similar.

Parameter	Symbol	Value
Active module length	L_{mem}	0.99 m
Active module radius	R	0.095 m
Central tube radius	R_c	0.02 m
Total membrane area	$A_{m,T}$	361 m^2
Fiber outer diameter	$d_{f,o}$	1.63x10^{-4} m
Fiber inner diameter	$d_{f,i}$	7.0x10^{-5} m
Water permeability coefficient	A	2.89x10^{-13} m/s-Pa
Salt permeability coefficient	B	8.12x10^{-10} m/s
Shell side inlet concentration	$C_{sh,i}$	35 kg/m^3
Shell side inlet gauge pressure	$P_{sh,in}$	5.5 MPa

Table 5.2: RO verification parameters [15].

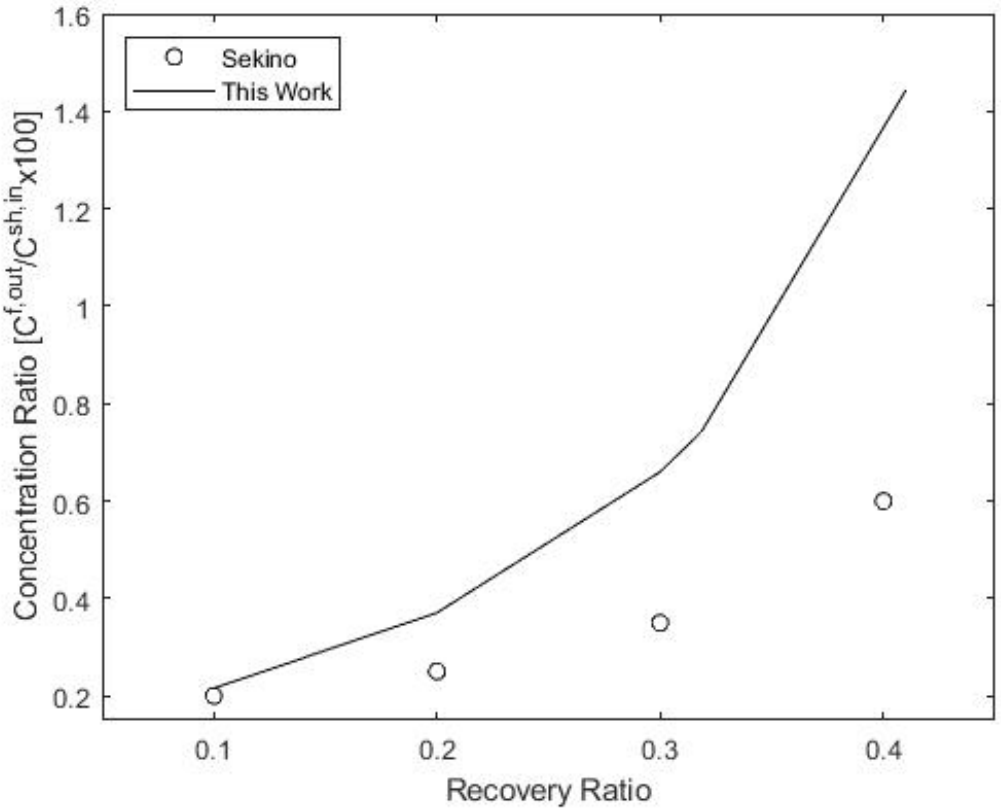

Figure 5.4: Ratio of produced freshwater concentration to inlet saltwater concentration for the RO module model presented in this report compared to experimental results by Sekino [15].

In Fig. 5.5, the flow rate of freshwater produced is indicative of the inlet flow rate of saltwater, as the recovery ratio mandates the ratio of the two. A lower flow rate of freshwater produced means there is lower inlet flow rate of saltwater. This means that, for the same recovery ratio, the fluid requires more time in contact with the membrane. This indicates that the model produced in this report simulates less efficient reverse osmosis.

Sekino uses a variable diffusion coefficient which could affect the discrepancy in results [15]. A paper by Sano & Mahidul indicates that this diffusion coefficient may be much higher than that used in this report [24]. A higher value for the diffusion coefficient would shift the results from the proposed model to more closely match the data from Sekino. The differing diffusion coefficient would also affect the derivation of the Sherwood number equation.

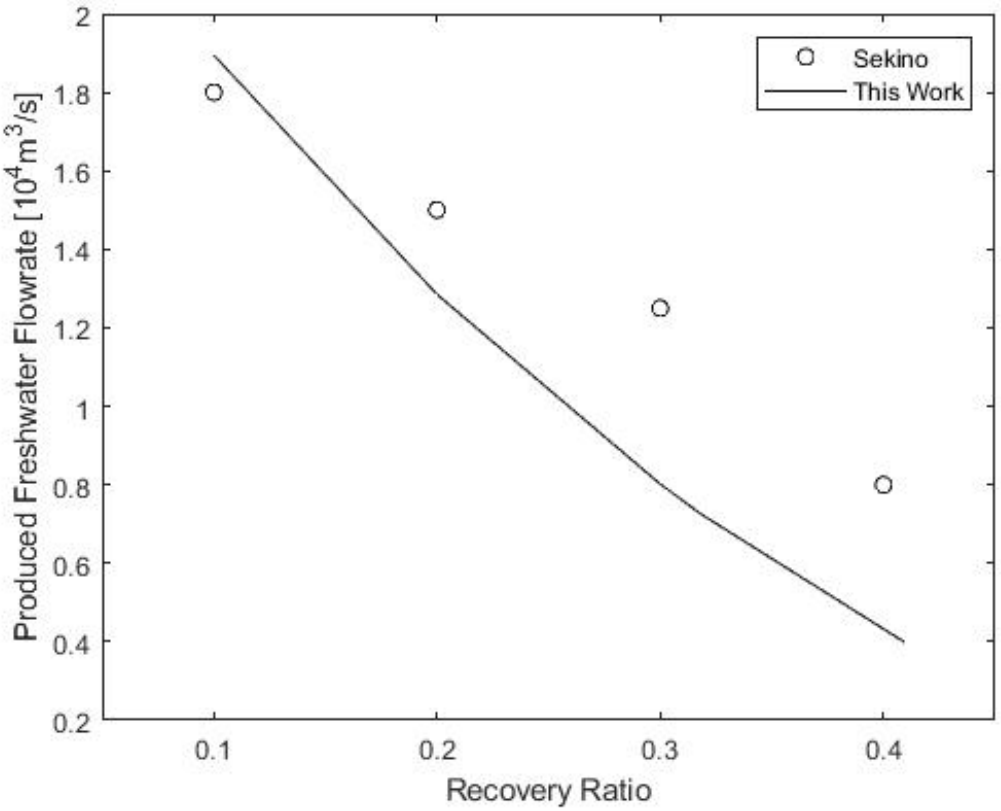

Figure 5.5: Flow rate of freshwater produced for the RO module model presented in this report compared to experimental results by Sekino [15].

Sekino also uses an osmotic pressure proportionary constant when calculating his water flux [15]. However, using a linear osmotic pressure in the proposed model only increased the difference in results.

5.2.2 Future Work

As discussed for the PRO module model in Sec. 5.1.9, improvements can be made to the RO module model. These are generally the same improvements: accounting for cross-winding of fibers; refining A and B; using a non-constant diffusion coefficient; creating a transient model. Deriving A and B with the equations used in this model is particularly relevant here due to the differences between this model and Sekino's.

Additionally, the Sherwood equation could be refined to more accurately reflect the flow conditions in the membrane module ultimately used in the OES system. As can be seen from comparing Tables 4.1 and 5.2, the membrane module used does have

different characteristics to the module in Sekino's research on which the Sherwood equation used was based [15]. Updating this equation would affect the concentration polarization and therefore the water and salt fluxes.

5.3 Pump & Turbine Models

As seen in Eq. 2.1, the work required by pumps and produced by turbines is necessary for calculating the OES system efficiency. Simple pump and turbine models were created with the assumption that the devices have constant efficiency. With this assumption, the power required for a pump is

$$\dot{W}^P = \frac{\dot{V}\Delta p}{\eta_P}, \tag{5.40}$$

and the work produced by a turbine is

$$\dot{W}^T = \eta_T \dot{V}\Delta p, \tag{5.41}$$

where $\dot{V}$ is the volumetric flow rate through the device and Δp is the magnitude of the pressure differential across the device. η_P and η_T are the efficiencies of the pump and turbine respectively. For the simulations detailed in this report, efficiencies of 90% were chosen for all pumps and turbines.

5.3.1 Future Work

Actual pumps and turbines have efficiencies that depend on the flow rates and differential pressures. If a specific pump or turbine is selected, a function for the efficiency can be implemented in the model to reflect this variable efficiency. However, the range of flow rates and pressure differentials the devices will see are required for selection of a suitable pump or turbine.

5.4 Pressure Exchanger Model

Pressure exchangers use a high pressure stream of fluid to pressurize a low pressure stream of equal flow rate. The pressure losses observed in pressure exchangers are approximately constant regardless of the pressure differential of the two streams.

For this reason, at high pressure differentials such as those seen in RO and PRO, a pressure exchanger is more efficient than a pump and turbine pair.

As mentioned in Chap. 4, pressure exchangers are utilized in both the RO and PRO stages of the proposed OES system. Fig. 5.6 shows a schematic of pressure exchanger with two fluid streams, A and B. Each of these streams have a pressure

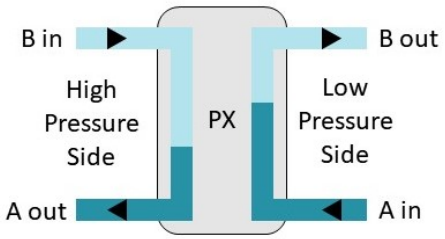

Figure 5.6: Pressure exchanger schematic.

and salinity at the inlet and outlet. The volumetric flow rates of the two streams are equal.

Due to the nature of pressure exchangers, the two streams come in direct contact with each other. This allows for some mixing of the streams. Therefore, the exiting streams will have a different salinity than the inlet streams. There is also some flow leakage used to lubricate the device. This leakage is neglected in this model.

As mentioned above, this model will assume a constant pressure drop in the pressure exchanger, regardless of flow conditions. This pressure drop, δp, is used to calculate the outgoing pressure for each stream:

$$p_{A,out} = p_{B,in} - \delta p, \tag{5.42}$$

$$p_{B,out} = p_{A,in} - \delta p. \tag{5.43}$$

This pressure drop is the reason booster pumps are required as detailed in Chap. 4. In this model, the pressure drop is set at 0.9 bar for both the high and low pressure sides of the pressure exchanger. This value was found as typical of some commercial pressure exchangers [20][19].

Pressure exchangers require equal volumetric flow rates for both streams. Equal mass flows were used in this model, neglecting the slight difference in density for different salinity streams. This assumption of equal mass flows allows for simple

calculation of the change in salinity. This is done through use of a mixing ratio, M:

$$M = \frac{s_{A,out} - s_{A,in}}{s_{B,in} - s_{A,in}}. \tag{5.44}$$

For this model, M was assumed to be constant at 0.058. This value was found by Stover et al. to be the value for the pressure exchanger they used when both streams had equal flow rates [20]. A mass balance of salt can then be used to determine the salinity of the remaining outlet flow:

$$s_{B,out} = s_{B,in} + s_{A,in} - s_{A,out}. \tag{5.45}$$

Note that salinities are used here because it is assumed that the total mass flow rates of each stream of fluid are equal.

5.4.1 Future Work

As discussed, there were some simplifying assumptions made during creation of the pressure exchanger model. These assumptions were a constant mixing ratio, a constant pressure drop, equal mass flow rates, and no leakage. Revising any of these assumptions would increase the accuracy of this model.

5.5 OES System Model

The component models described above were combined to create an OES system model. The OES model begins with a given mass of saltwater and no freshwater or concentrated brine in their respective tanks. This saltwater is then completely separated using RO. The resulting freshwater and brine are then completely used up in the PRO stage, completing the cycle. A full cycle was used so that the efficiency of the system could be easily evaluated, as detailed in Sec. 2.3. The model could, however, be modified to perform partial cycles.

This model neglects pressure losses in pipes as well as any temperature changes within the system.

5.5.1 RO Stage

The model begins by running the RO stage. The inputs required for this stage are the inital masses and salinities of fluid in the saltwater, freshwater and brine tanks. As noted above, for this report the initial masses of freshwater and brine were set to zero. The inlet and outlet pressures for the saltwater side are also inputs.

The time step is the last input. For the RO stage, the only input to the module model that changes between time steps is the concentration due to mixing in the pressure exchanger. For this report, a time step of 30s was chosen for the RO stage. This was the approximate time it takes the saltwater to flow through the membrane, for operating conditions typical of those simulated in this report. This could be altered to dynamically adjust to reflect the flow rate during each iteration.

At the beginning of each iteration, the RO module model is run using the pressures and inlet salinity as inputs. For the first iteration the inlet salinity is simply that of the saltwater tank. For subsequent iterations, this is calculated using the pressure exchanger model.

The change in mass and salinity in the saltwater, freshwater and brine tanks are then calculated. The work required for the pumps is also calculated for each iteration and added to the total RO work. This is repeated for each iteration until there is no fluid remaining in the saltwater tank.

The model can be split into separate stages for easy optimization of each stage. If just the RO stage is desired, the model ends here. If the total OES system is desired, the model continues onto the PRO stage. If only the PRO stage is desired, the model will require the appropriate inputs for the PRO stage to be manually entered.

5.5.2 PRO Stage

With the RO stage complete (or if simulating the PRO stage alone), the saltwater tank is now empty and the freshwater and brine tanks have values for the mass and salinity of the fluids they contain. In addition to these values, the inlet and outlet pressures on the shell side and the inlet pressure on the fiber side of the PRO module are required. As mentioned in Sec. 5.1, all pressures are gauge pressures relative to the outlet pressure on the fiber side which is therefore set to 0.

Similarly to the RO stage, a time step for the iterations is required. A value of 20s was chosen using the same method as above. If the configuration with no freshwater recirculation is used, then the salinities from the pressure exchanger are

the only inputs to the module model that change each time step. If, however, the fiber side outlet is recirculated back into the freshwater tank, the salinity of the incoming freshwater also changes.

This portion of the model functions in much the same matter as the RO stage. The PRO module model is run using the pressures and inlet salinities of the freshwater and brine as inputs. For the first iteration, the inlet brine salinity is simply that of the brine tank. For subsequent iterations, this is calculated using the pressure exchanger model.

The change in mass and salinity in the saltwater, freshwater and brine tanks are then calculated. The outlet flow from the shell side is split into two streams. One passes through the pressure exchanger and the other passes through the turbine. They are both then combined and added to the saltwater. The addition of the flow from the pressure exchanger to the saltwater tank is delayed by one time step. That is, the outlet flow is passed into the pressure exchanger for the subsequent time step and before being added to the saltwater tank. For the configuration with no freshwater recirculation the outlet flow from the fiber side is simply added to the saltwater tank as seen in Fig. 4.2. For the configuration with recirculation shown in Fig. 4.3, this outlet flow is added back to the freshwater tank and the tank's salinity is recalculated.

The work required for the pumps and produced by the turbine is also calculated for each iteration and added to the total PRO work. This is continued for each iteration until there is no fluid remaining in one or both of the freshwater and brine tanks. If there is fluid remaining in one of these tanks, it is simply added to the saltwater tank without passing through the PRO module at the end of the cycle.

With the work required for the RO stage and the work produced by the PRO stage, the system efficiency is calculated. Potential future improvements to the overall OES model are discussed in Sec. 6.3.1.

Chapter 6

Results & Discussion

The models discussed above were run and preliminary results were produced. It is important to note that only a handful of scenarios were run. The results presented here give an indication of how the proposed OES system could perform but the operating parameters are by no means optimized.

As mentioned in Sec. 5.5, the proposed model simulates complete cycles of the OES system. That is, during the RO stage all of the saltwater is separated. Then, in the PRO stage, the resulting brine and freshwater are combined until one tank is empty, then any fluid remaining in the other tank is added back to the saltwater tank. This allows for simple calculation of system efficiency, but real operation would not always be in this manner.

The design of the OES model created is such that it can be easily split into separate models for the RO and PRO stages. This reduces model run times and allows each stage to be optimized individually. Therefore, an RO stage model was run for a variety of operating conditions, and then the most promising results from this stage were used as inputs for the PRO stage which was then run at various operating conditions.

The RO stage was run such that target recovery ratios were achieved. Recovery ratio, RR, is

$$RR = \frac{\dot{V}_{f,o}}{\dot{V}_{sw,i}}, \tag{6.1}$$

where $\dot{V}_{f,o}$ is the outgoing flow rate of freshwater and $\dot{V}_{sw,i}$ is the inlet flow rate of saltwater to the RO module. A recovery ratio of 0.5 would achieve approximately equal outgoing flow rates of freshwater and brine, while a recovery ratio of 0.3 would

produce less freshwater and more brine at lower salinity.

6.1 Model Inputs

Initial operating conditions were required to begin running the model. The first decision to be made is the concentration of the initial saltwater. RO typically uses either brackish water or seawater for its intake. PRO typically uses seawater or a concentrated brine for the high salinity inlet. A higher salinity water requires less tank volume for the same theoretical energy storage, resulting in higher energy density. Therefore, a solution with a salinity of 35g-salt/kg-solution was used, similar to seawater. This allowed RO to function with seawater-like salinity as the input, and the PRO used the resulting high salinity brine.

A small amount of working fluid was used for these simulations, only 10 kg of initial saltwater. This small amount allows for faster simulations and doesn't affect the RO stage or the PRO stage with the no recirculation configuration significantly. The only changes to these stages are the salt leakage through the PX, which are relatively minor and have begun to approach equilibrium by the end of even these small cycles. For the RO stage of one OES cycle, the inlet saltwater salinity changed by 1.6% over the course of the cycle and the change between the final two iterations was less than 0.1%. The PRO stage with no freshwater recirculation produced similar salinity changes, so the system is approaching steady state with this small mass of working fluid.

For the PRO stage with recirculation, the salinity of the freshwater is constantly changing. This affects the salinity of the outlet flows and therefore the salinity of the brine leaving the pressure exchanger. There is no steady state operation for this configuration. A larger working fluid mass would lead to smaller incremental changes in salinity for the same time step. However, a good idea of the effects of changing freshwater salinity on the work produced is achieved with 10kg of working fluid.

For PRO, the pressure of the draw solution was set at half the osmotic pressure of the brine. For an ideal system with constant feed pressure, this is the pressure which would produce the maximum amount of work for a given amount of working fluid [1][6].

The ideal system pressure for RO is not as simply calculated, especially in the context of an OES system. Therefore a somewhat arbitrary decision was made. For the RO stage, the saltwater inlet pressure was chosen to be twice the osmotic pressure

of the saltwater in the tank, i.e. 51.8 bar. Additionally, for the case of a recovery ratio of 0.5, several pressures were tested, from 2 up to 3 times the osmotic pressure of the saltwater. 3 times the osmotic pressure is 77.7 bar, which is above the working pressure of most membrane modules. This is of interest to determine if modules that can withstand higher pressures are desirable.

6.2 Results

For the RO stage, the simulation was run to achieve recovery ratios of 0.3, 0.4, 0.5 & 0.6. Results can be seen in Table 6.1. The salinity of the exiting freshwater, $s_{fw,o}$, is

$P_{sw,i}$	RR	$s_{fw,o}$ [g/kg]	η_{RO}
$2\pi_{sw}$	0.3	4.5	38.8%
$2\pi_{sw}$	0.4	7.1	35.3%
$2\pi_{sw}$	0.5	10.3	30.6%
$2\pi_{sw}$	0.6	13.9	25.9%

Table 6.1: Simulation results for RO stage at various recovery ratios.

noted as it is an indication of the quality of separation and the energy potential for the PRO stage. Trials for a range of saltwater inlet pressures, $P_{sw,i}$, were also run for the case of a recovery ratio of 0.5. Results are shown in Table 6.2.

$P_{sw,i}$	RR	$s_{fw,o}$ [g/kg]	η_{RO}
$2\pi_{sw}$	0.5	10.3	30.6%
$2.1\pi_{sw}$	0.5	9.7	30.8%
$2.2\pi_{sw}$	0.5	9.2	30.8%
$2.3\pi_{sw}$	0.5	8.8	30.5%
$2.4\pi_{sw}$	0.5	8.4	30.3%
$2.5\pi_{sw}$	0.5	8.0	30.1%
$2.6\pi_{sw}$	0.5	7.6	30.1%
$2.7\pi_{sw}$	0.5	7.3	29.7%
$2.8\pi_{sw}$	0.5	7.0	29.4%
$2.9\pi_{sw}$	0.5	6.7	29.1%
$3\pi_{sw}$	0.5	6.5	28.6%

Table 6.2: Simulation results for RO stage at a range of pressures.

The PRO stage was first run with inputs from a RR of 0.3 in the RO stage as this had the highest RO stage efficiency and high quality freshwater. For the PRO stage with no recirculation, trials were also run at a RR of 0.5. Results for

the highest efficiency cases are shown in Table 6.3. The first column indicates which PRO configuration was used for the simulation. $P_{br,i}$ is the pressure at which the brine entered the PRO module, while $P_{sw,i}$ is for the saltwater entering the RO module. $m_{fw,f}$ is the mass of fluid in the freshwater tank at the end of the PRO cycle, while $m_{br,f}$ indicates the final mass in the brine tank.

FW Recirc.	$P_{br,i}$	$P_{sw,i}$	RR	$m_{fw,f}$ [kg]	$m_{br,f}$ [kg]	η_{PRO}	η_{OES}
Yes	$0.5\pi_{br}$	$2\pi_{sw}$	0.3	1.08	0	18.4%	7.13%
No	$0.5\pi_{br}$	$2\pi_{sw}$	0.3	0	2.39	23.1%	8.97%
No	$0.5\pi_{br}$	$2\pi_{sw}$	0.5	0	0.06	18.1%	6.11%
No	$0.5\pi_{br}$	$2.2\pi_{sw}$	0.5	0.03	0	22.0%	6.77%
No	$0.5\pi_{br}$	$3\pi_{sw}$	0.5	0.03	0	25.9%	7.41%

Table 6.3: Simulation results for overall OES system.

The work produced for each iteration of the PRO stage for the freshwater recirculation configuration is shown in Fig. 6.1. This is for the run detailed in the first row of Table 6.3. The work produced in the final iteration was negative. Therefore, the work from this iteration was not included in the net work for the stage used to calculate system efficiency. This is acceptable as the remaining fluid in the tank could have simply been transferred to the saltwater tank without reducing the total work produced, neglecting pipe losses. The salinity of the freshwater entering the PRO module for this run of the model can be seen in Fig. 6.2.

6.3 Discussion

The overall OES system efficiencies achieved aren't very promising, with the highest value being just below 9%. However, these are just initial results and the operating parameters have not been optimized. Focusing on the individual stage efficiencies gives an idea of where to focus optimization efforts. Neither stage achieved particularly high efficiencies, with the RO stage topping out at 38.8% and the PRO stage at 25.9%.

For the RO stage, lower recovery ratios lead to higher efficiency. For equal feed pressures, a lower recovery ratio requires the fluid to spend less time in the membrane module. This gives less time for salt to cross the membrane. Lower average shell side salinity also accounts for this lower total salt transfer. Spending less time in the membrane module is also proportional to increased flow rates. Increased flow rates

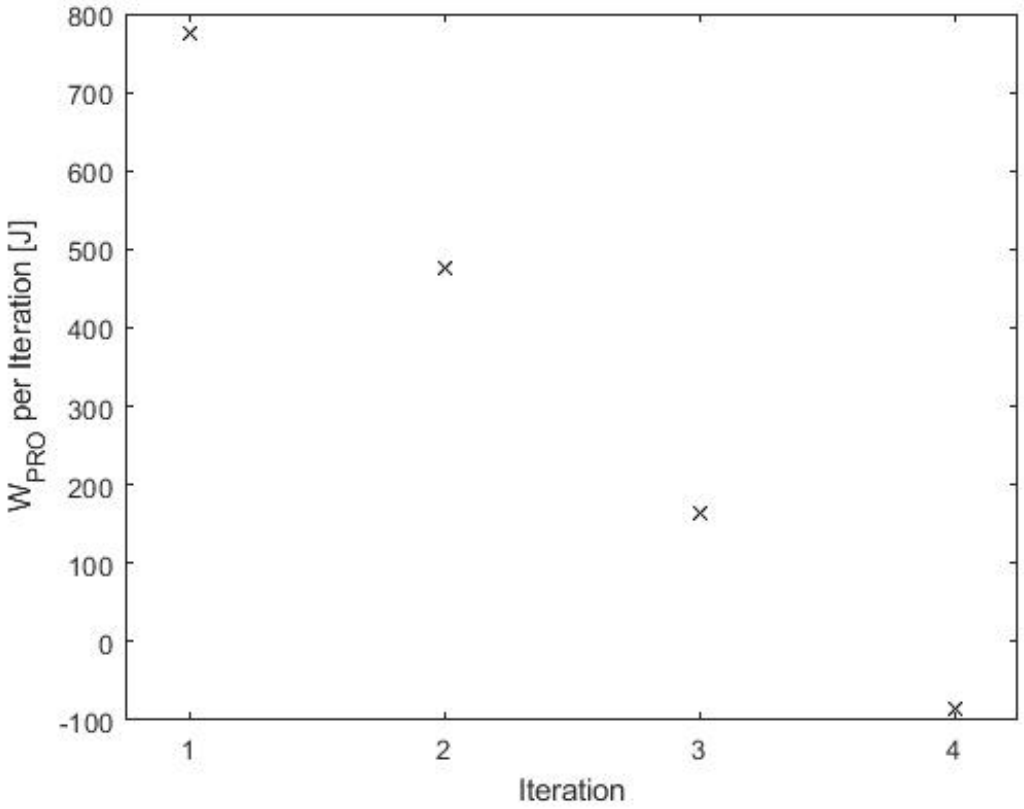

Figure 6.1: Work produced for each iteration of the model by the PRO stage with freshwater recirculation.

decrease external concentration polarization, increasing efficiency.

Looking at the values in Table 6.2, the effects of changing shell side pressure on the RO stage operation can be seen. Higher pressure leads to higher water flux which increases concentration polarization and therefore increases losses. However, lower pressures require the solution to spend more time in the membrane module. This allows more time for salt to cross the membrane and results in a higher freshwater salinity. This reduces the work potential for the PRO stage. In terms of efficiency of the stage alone, the maximum values, 30.8%, is found at a pressure of 2.1bar or 2.2bar.

For the operating conditions explored, the PRO configuration with no freshwater recirculation performed best, achieving an overall OES system efficiency of 8.97%. The configuration with recirculation only resulted in an OES efficiency of 7.13% with the same input conditions. This is likely because there is more room for optimization

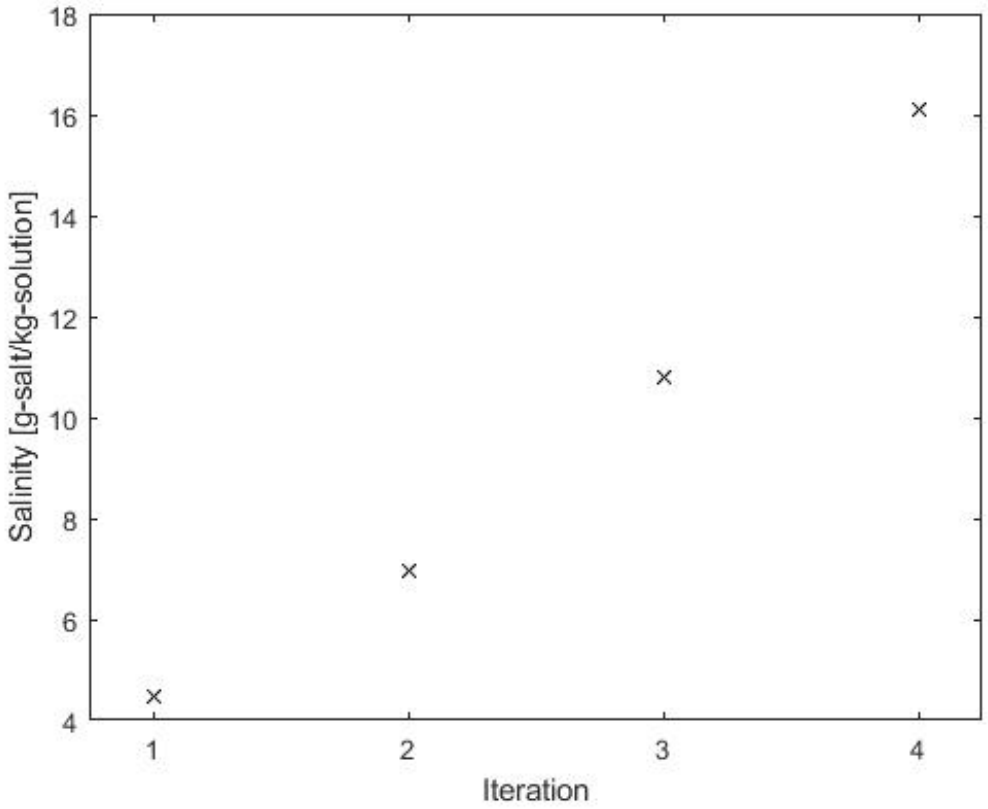

Figure 6.2: Freshwater salinity for each iteration of the model for the PRO stage with freshwater recirculation.

in the configuration with recirculation. Potential improvements are discussed in Sec. 6.3.1.

Since the highest efficiency PRO stage with and without freshwater recirculation both have the same initial conditions, the difference in efficiency is directly proportional to a difference in work produced. For the configuration with recirculation, the work output for each iteration is illustrated in Fig. 6.1. By the final iteration, work produced is negative, meaning the PRO stage consumes more power than it produced. The power required for pumping is greater than that produced by the turbine. This is due to the lower water flux in subsequent iterations. The volume flow of water passing across the membrane is the flow rate which passes through the turbine. The lower flux is due to higher freshwater salinity as seen in Fig. 6.2. Higher freshwater salinity reduces the osmotic pressure difference which is the driving force in PRO.

The configuration with freshwater circulation will always have fluid in the fresh-

water tank at the end of the cycle. For the configuration with no-recirculation, an attempt was made to balance the flows such that the freshwater and brine were utilized as much as possible. This led to the highest efficiencies for a given flow rate of brine. In the case of a 0.3 RR, there was so much excess brine that it was not able to be fully consumed. As the flow rate of freshwater was reduced to attempt to use up all of the brine, the ratio of water flux to freshwater flow rate became too high, preventing the model from converging on a solution. The flow rate of the incoming brine was adjusted and, despite a large mass of brine remaining, this was found to be optimal. Higher flow rates of brine that left less fluid in either tank at the end of the cycle resulted in lower efficiencies.

A higher efficiency for the PRO or RO stage alone doesn't necessarily lead to the highest overall OES system efficiency. This can be seen in the last two rows of Table 6.3. The second last row used operating conditions for the RO stage that resulted in the highest RO stage efficiency for a recovery ratio of 0.5. Despite this, it achieves a lower system efficiency than the last row. This is because the lower freshwater salinity provides more work potential for the PRO stage. The PRO stage then achieves a higher efficiency which makes up for the reduced RO stage efficiency.

On the PRO side, the second row in Table 6.3 achieves a lower PRO stage efficiency than the last row. However, the RO stage is more efficient, resulting in a higher OES system efficiency.

Fig. 6.1 and Fig. 6.2 show the importance of salt leakage, especially for the configuration with freshwater recirculation. In just four iterations, the salinity of the freshwater increases nearly four times and the work produced decreases from about 800 J per iteration to nearly -100 J per iteration. The impact of salt leakage is also seen by looking at the results in Tables 6.2 and 6.3. Despite higher efficiency of the RO stage at an incoming saltwater pressure of $2.2\pi_{sw}$, the simulation with a saltwater pressure of $3\pi_{sw}$ yields a higher overall efficiency. This is due to the much lower salinity of the freshwater produced for the latter simulation. The fluid has spent less time in contact with the membrane so allowed less time for salt to pass across the membrane, resulting in higher quality freshwater. This lower salinity freshwater enables higher efficiency PRO. If there was less salt leakage, higher cycle efficiencies would be able to be achieved for all operating conditions.

This report only examines the overall system efficiency. Other metrics such as power per membrane area or energy stored per mass of working fluid were not explored. If an OES system was to be built, these other metrics would need to be

accounted for and factored into optimization.

6.3.1 Future Work

As noted above, operating conditions were not optimized in this work. This is a key area in which improved results can be found. These operating conditions include pressures, recovery ratios and the initial saltwater salinity. Optimizing these parameters will result in improvement of the system efficiency.

Additionally, the system design and operation can be improved. For the PRO configuration with freshwater recirculation, beyond simply testing more operating conditions, the shell side pressure could change during the course of a cycle. As the salinity of the freshwater increases, the difference in osmotic pressures decreases. It follows that the hydraulic pressure differential should decrease as well.

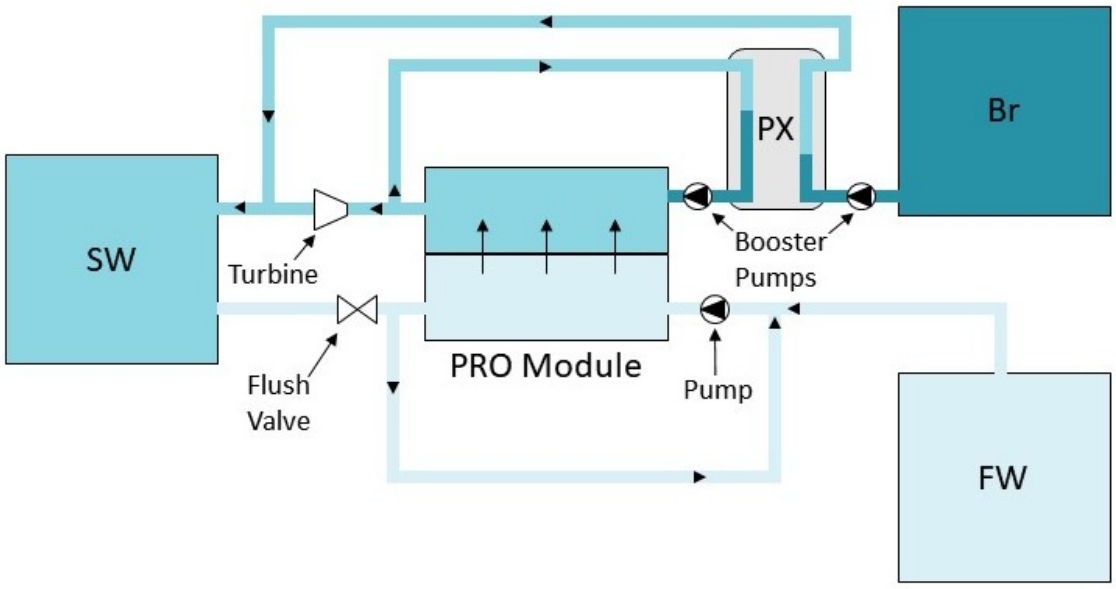

Figure 6.3: Alternate PRO stage configuration with freshwater recirculation.

Alternate PRO configurations could also be used. Instead of recirculating the freshwater back into the freshwater tank, it could simply be recirculated directly into the PRO module as shown in Fig. 6.3. Water that passes to the shell side within the PRO module is replaced by water from the freshwater tank. This configuration would allow for more control of the salt build up on the freshwater side. It would however require additional optimization of the flushing. The freshwater recirculation

could be flushed periodically, a portion could constantly be bled out and fed into the saltwater tank or some combination of the two methods.

Similar to the system proposed by Bharadwaj & Struchtrup [5], the OES system could be expanded to have multistage RO and/or PRO. This would increase system complexity and cost, but could help to increase the system efficiency.

The system presented in this report uses the same membrane module for RO and PRO. This allows for reduced system cost and complexity. However, if a membrane module specifically designed for RO and a separate one for PRO are used, there could be efficiency gains available.

Potential improvements to the component models are detailed in the various future work sections in Chap. 5.

Chapter 7

Conclusions

This report explored the creation of an OES system model. Osmotic energy storage has the potential to aid in the world's shift to clean energy, helping mitigate the issues with variability in the production of clean energy such as wind and solar.

Bharadwaj & Struchtrup proposed an OES system which uses pressure retarded osmosis and reverse osmosis in a closed energy storage system [5]. However, their analysis used a few key simplifying assumptions. This report outlined the creation of a thermodynamics based OES model in MATLAB that can more accurately assess the promise of such a system, without need for these assumptions.

Preliminary results were found, with a maximum round trip efficiency of 8.97%. Operating conditions were not optimized and higher efficiencies can no doubt be achieved. This efficiency was found using a configuration for PRO with no freshwater recirculation, outflow from the fiber side of the membrane module simply went to the saltwater tank. A PRO stage configuration with recirculation achieved a round trip efficiency of 7.13%. However, the recirculation configuration could greatly benefit from improvements to system operation and optimization of operating conditions. Salt leakage was found to be a major factor in limiting system efficiency, especially for the configuration with freshwater recirculation.

Appendix A

PRO Verification Results

This appendix includes plots of additional results for the PRO module model verification. As discussed in Sec. 5.1.8, the error varies from 0.2% to 24.1%. The results here are for different inlet flowrates, noted in the figure captions.

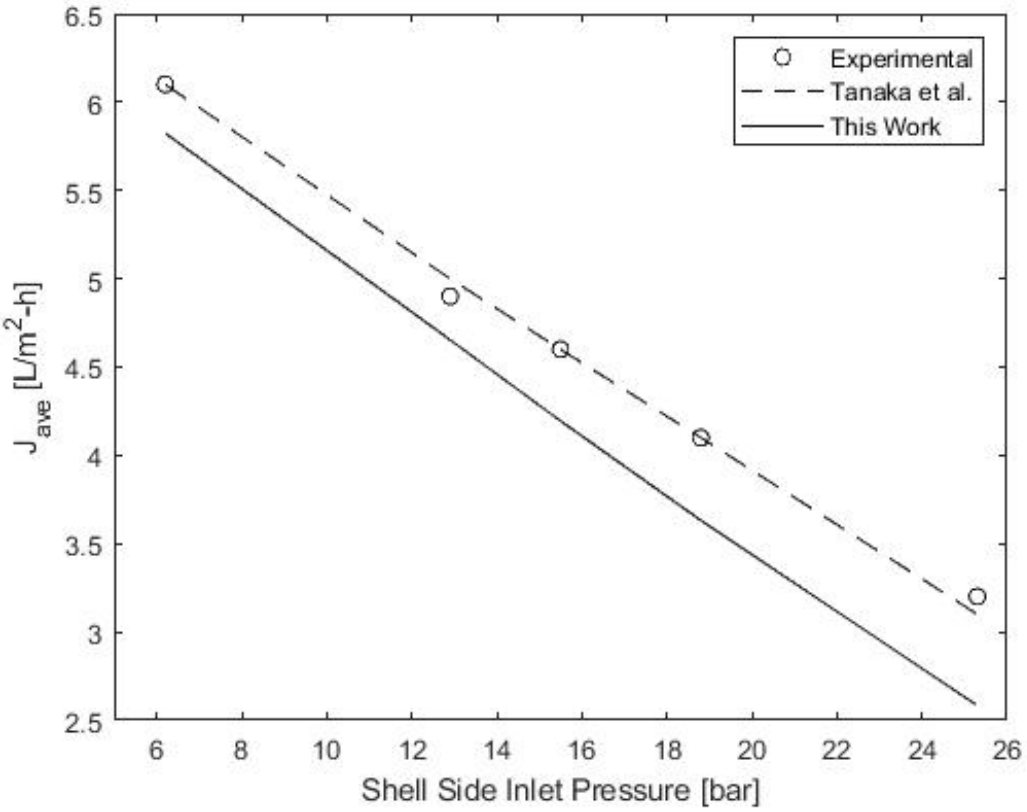

Figure A.1: Results from the PRO module model presented in this report compared to experimental and simulated results by Tanaka et al. [25]. Data is for entering flowrates of 8 lpm for high salinity water and 10 lpm for freshwater.

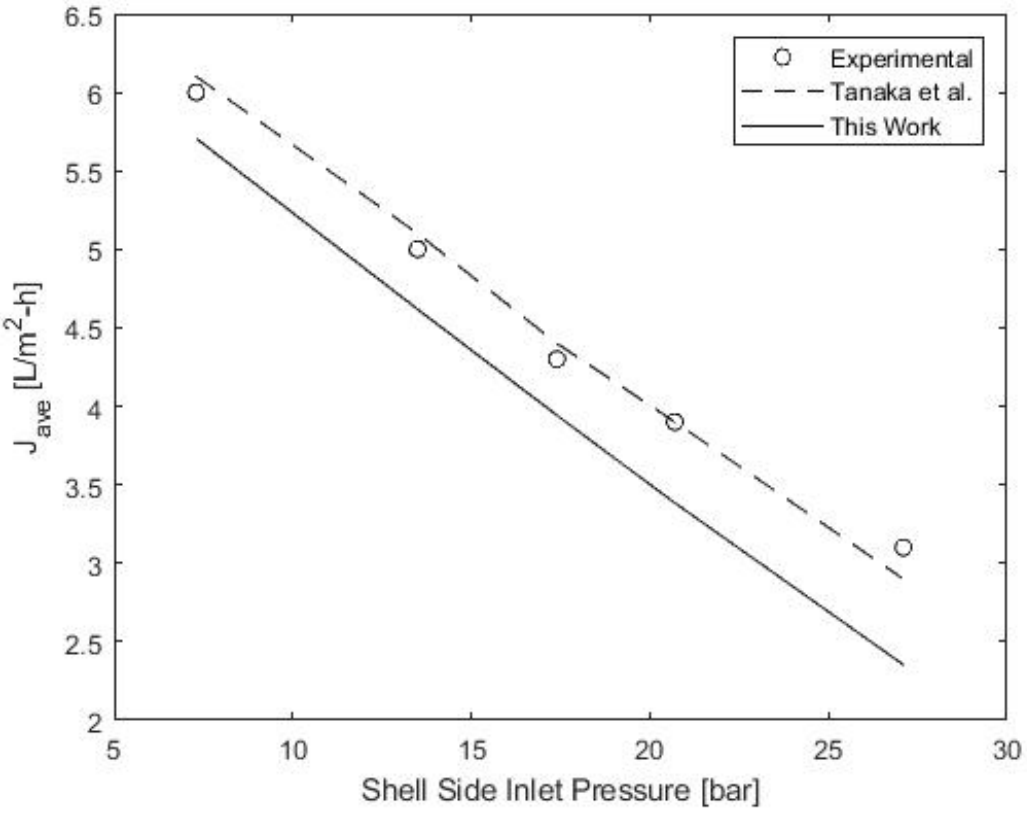

Figure A.2: Results from the PRO module model presented in this report compared to experimental and simulated results by Tanaka et al. [25]. Data is for entering flowrates of 8 lpm for high salinity water and 12 lpm for freshwater.

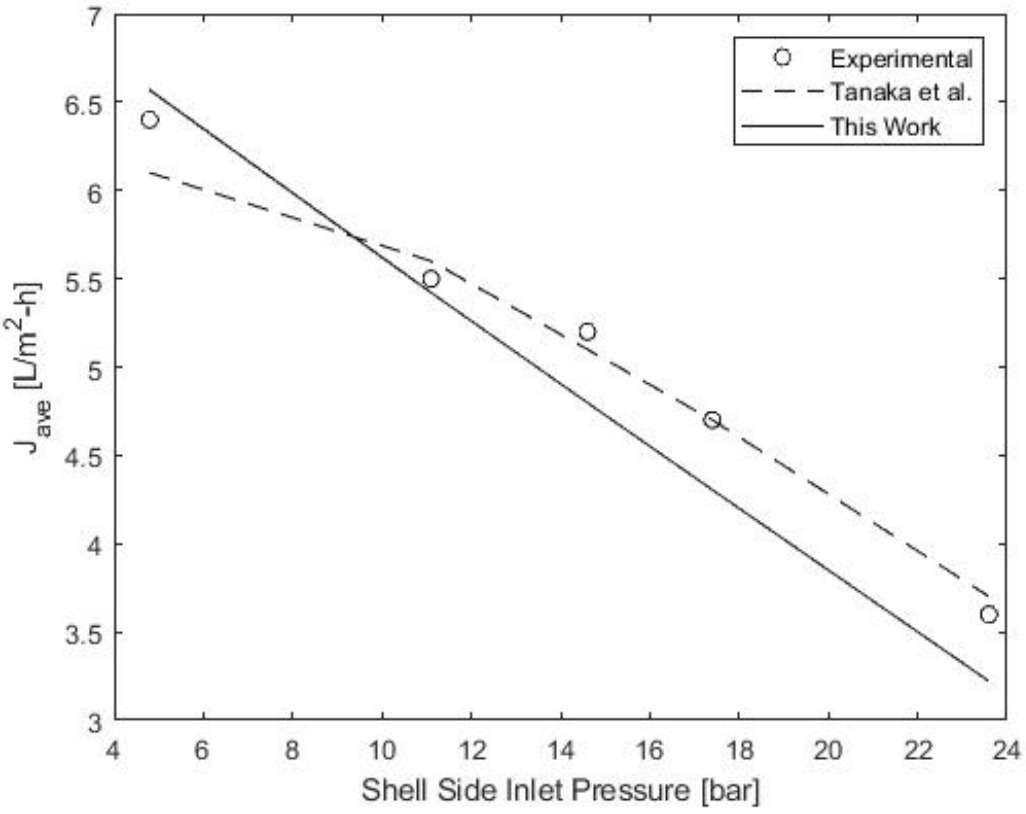

Figure A.3: Results from the PRO module model presented in this report compared to experimental and simulated results by Tanaka et al. [25]. Data is for entering flowrates of 12 lpm for high salinity water and 8 lpm for freshwater.

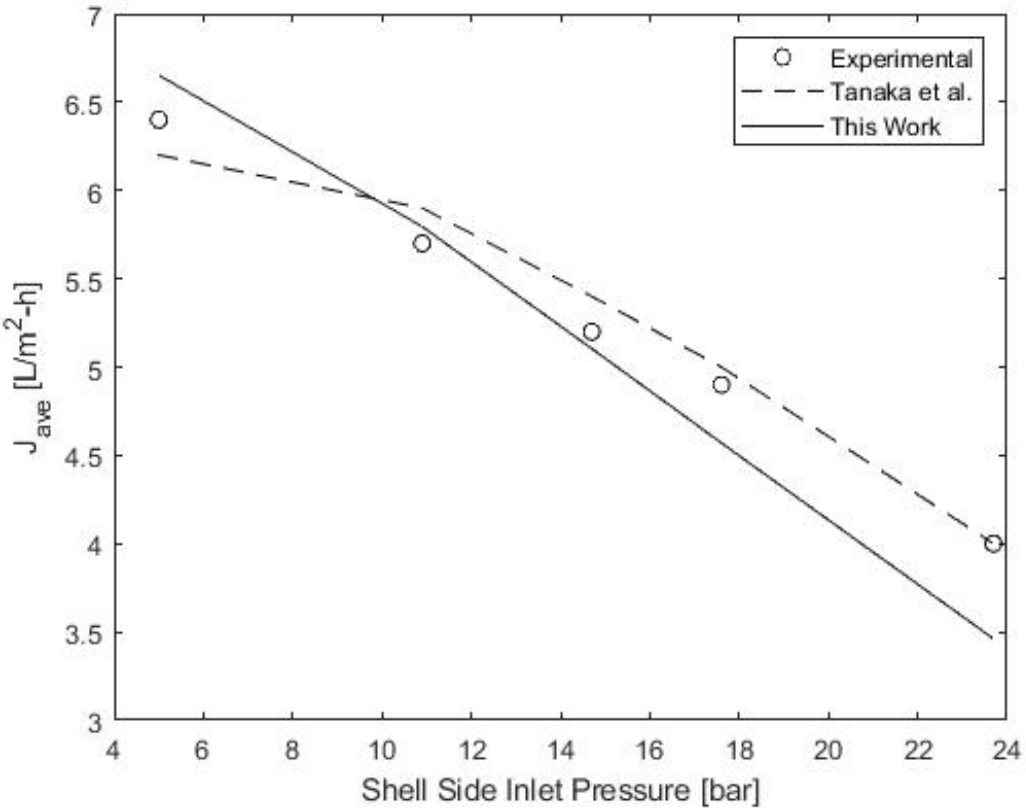

Figure A.4: Results from the PRO module model presented in this report compared to experimental and simulated results by Tanaka et al. [25]. Data is for entering flowrates of 16 lpm for high salinity water and 8 lpm for freshwater.

Bibliography

[1] Achilli A. and Childress A.E. Pressure retarded osmosis: From the vision of Sidney Loeb to the first prototype installation - Review. *Desalination*, 261, 2010.

[2] Achilli A., Cath T.Y., and Childress A.E. Power generation with pressure retarded osmosis: An experimental and theoretical investigation. *Journal of Membrane Science*, 343:42–52, 2009.

[3] Kumano A. and Matsuyama H. Analysis of Hollow Fiber Reverse Osmosis Membrane Module of Axial Flow Type. *Journal of Applied Polymer Science*, 123:463–471, 2012.

[4] Klaysom C., Cath T.Y., Depuydt T., and Vankelecom I.F.J. Forward and pressure retarded osmosis: potential solutions for global challenges in energy and water supply. *Chem. Soc. Rev.*, 42:6959–6989, 2013.

[5] Bharadwaj D. and Struchtrup H. Large scale energy storage using multistage osmotic processes: Approaching high efficiency and energy density. *Sustainable Energy & Fuels*, 1(3):599–614, 2017.

[6] Bharadwaj D., Fyles T., and Struchtrup H. Multistage Pressure-Retarded Osmosis. *Journal of Non-Equilibrium Thermodynamics*, 41(4):327–347, 2016.

[7] Sivertsen E., Holt T., and Thelin W. Concentration and Temperature Effects on Water and Salt Permeabilities in Osmosis and Implications in Pressure-Retarded Osmosis. *Membranes*, 8(3), 2018.

[8] Sivertsen E., Holt T., Thelin W., and Brekke G. Pressure retarded osmosis efficiency for different hollow fibre membrane module flow configurations. *Desalination*, 312:107–123, 2013.

[9] Palacin L. G. *Modelling, simulation and advanced control of small-scale reverse osmosis desalination plants*. PhD thesis, University of Vallodiolid, 2014.

[10] Struchtrup H. *Thermodynamics and Energy Conversion*. Springer-Verlag, Heidelberg, 2014.

[11] Wijmans J.G. and Baker R.W. The solution-diffusion model: a review. *Journal of Membrane Science*, 107:1–21, 1995.

[12] Nayar K., Sharqawy M., Banchik L., and Lienhard J. Thermophysical properties of seawater: A review and new correlations that include pressure dependence. *Desalination*, 390:1–24, 2016.

[13] Lee K.L., Baker R.W., and Lonsdale H.K. Membranes for power generation by pressure-retarded osmosis. *Journal of Membrane Science*, 8:141–171, 1981.

[14] Kishimoto M., Tanaka Y., Yasukawa M., Goda S., Higa M., and Matsuyama H. Optimization of Pressure-Retarded Osmosis with Hollow-Fiber Membrane Modules by Numerical Simulation. *Industrial & Engineering Chemistry Research*, 58:6687–6695, 2019.

[15] Sekino M. Study of an analytical model for hollow fiber reverse osmosis module systems. *Desalination*, 100, 1995.

[16] Sharqawy M., Lienhard J., and Zubair S. Thermophysical properties of seawater: a review of existing correlations and data. *Desalination and Water Treatment*, 16:354–380, 2010.

[17] Shibuya M., Yasukawa M., Goda S., Hidehiko S., Takahashi T., Higa M., and Matsuyama H. Experimental and theoretical study of a forward osmosis hollow fiber membrane module with a cross-wound configuration. *Journal of Membrane Science*, 504, 2016.

[18] Yip N.Y., Tiraferri A., Phillip W.A., Schiffman J.D., Hoover L.A., Kim Y.C., and Elimelech M. Thin-film composite pressure retarded osmosis membranes for sustainable power generation from salinity gradients. *Environ. Sci. Tech.*, 45:4360–4369, 2011.

[19] Stover R. Saltwater reverse osmosis with isobaric energy recovery devices. *Desalination*, 203, 2007.

[20] Stover R., Fernandez A., and Galtes J. Permeate Recovery Rate Optimization at the Alicante Spain SWRO Plant. International Desalintation Association World Congress: Dubai 2009 DB09-083.

[21] Sarp S., Li Z., and Saththasivam J. Pressure Retarded Osmosis (PRO): Past experiences, current developments, and future prospects. *Desalination*, 389:2–14, 2016.

[22] Holt T., Sivertsen E., Thelin W., and Brekke G. *Pressure Dependency of the Membrane Structure Parameter and Implications in Pressure Retarded Osmosis (PRO)*, chapter 6. Books on Demand, 2018.

[23] Lobo V. Mutual diffusion-coefficients in aqueous electrolyte solutions. *Pure and Applied Chemistry*, 65:2614–2640, 1993.

[24] Sano Y. and Mahidul I. Optimum operating condition of a hollow fiber reverse osmosis desalination system. *Cogent Engineering*, 5, 2018.

[25] Tanaka Y., Yaukawa M., Goda S., Sakurai H., Shibuya M., Takahashi T., Kishimoto M., Higa M., and Matsuyama H. Experimental and simulation studies of two types of 5-inch scale hollow fiber membrane modules for pressure-retarded osmosis. *Desalination*, 447:133–146, 2018.